Received: 6 May 2020 | Revised: 7 July 2020 | Accepted: 7 July 2020

DOI: 10.1002/pcr2.10144

FULL PAPER

Polymer Crystallization WILEY

An enhanced phase field model for the numerical simulation of polymer crystallization

Amine Bahloul[1,2] | Issam Doghri[1,2] | Laurent Adam[2]

[1]Université Catholique de Louvain, Institute of Mechanics, Materials and Civil Engineering, (IMMC), Louvain-la-Neuve, Belgium

[2]e-Xstream Engineering Sarl (Part of Hexagon Manufacturing Intelligence), Bascharage, Luxembourg

Correspondence
Issam Doghri, Université Catholique de Louvain, Institute of Mechanics, Materials and Civil Engineering, (IMMC), Bâtiment Euler, 4 Avenue G. Lemaître, B-1348 Louvain-la-Neuve, Belgium.
Email: issam.doghri@uclouvain.be

Funding information
e-Xstream engineering sarl (part of Hexagon Manufacturing Intelligence); Fonds National de la Recherche Luxembourg

Abstract

An enhanced phase field model is proposed for the numerical simulation of crystallization in semicrystalline polymers. As with other models, it is based on coupling the heat equation with the Alle–Cahn equation, which is derived from the Gibbs–Thomson solid–liquid interface equation. Starting from spherulite nucleation, existing phase field models can simulate their evolution in a surrounding liquid and separate the amorphous and crystalline phases. However, the predictions of the morphological characteristics of the spherulites remain qualitative only. Moreover, the predicted spherulite evolution as a function of crystallization temperature is not consistent with experimental results. In this work, existing phase field models are enhanced in order to obtain experimentally consistent results. We target these characteristics to make them quantitative: spherulite growth, crystal morphology, and crystalline rate in spherulite. We show the importance of modeling the dependence of the model's parameters with respect to crystallization temperature, because, if assumed constants, the predicted results are not consistent with polymers physics. The model is numerically implemented using the finite difference method in a research version of the Digimat software so that 2D and 3D simulation results are presented and compared to experimental data, illustrating the quantitative adequacy of the predictions with experimental evidence.

KEYWORDS

amorphous, crystalline, crystallization, growth, nucleation, phase field model, polymer, spherulite

1 | INTRODUCTION

Polymeric materials are widely used in the industry, which explains the existence of several manufacturing processes, such as plastic injection molding, plastic blowing, and more recently 3D printing, and so on. Nowadays, the industry tends to digitize these processes, in order to provide information on the mechanical strength and final shape of the sample before starting production, the final aim being to optimize the process and reduce costs. In order to model the constitutive response of the polymers, a thermomechanical modeling based on viscoelasticity and/or viscoplasticity can be used, such as in refs. [1,2]. But such models remain insufficient because after melting, the material will undergo a very important phenomenon which is crystallization. Variation in crystalline rate will lead to material inhomogeneity at the micro scale, which will change the behavior from one region to another. So the objective of this study is to understand this phenomenon and to model it.

Crystallization in polymers is the rearrangement of molecular chains to form ordered regions. It occurs below the melting temperature and above the glass transition temperature. Molecular chains fold to form lamellae. These lamellae originate from a single nucleation to give at the end a spherical structure called spherulite or a disc if the sample is very thin[3] and it can take other forms if the polymer crystallizes under shear conditions[4]. Spina et al.[4] show also that the shear

conditions accelerate the crystallization process. There are three stages in crystallization. The first is nucleation, it is the creation of primary nuclei.[5] Next, a period of rapid growth of spherulites is called primary crystallization. Finally, secondary crystallization is a slower crystallization period that occurs once the spherulites have come into contact. Yokota and Kawakatsu[5] propose two nucleation theoretical models, for single and multiple chain systems, respectively, which can be used with a phase field model to simulate polymer crystallization. There is another mechanism called spinodal decomposition, which is a thermodynamic phase decomposing into two phases, when there is no nucleation barrier. The nucleation process results from a first-order phase transition, while the spinodal decomposition process is an example of second-order phase transition[6].

In the spherulite, there are two phases, amorphous and crystalline, the quantity of each state depends essentially on the crystallization temperature. The amorphous state is characterized by the random configuration of molecular chains, this structure gives the polymer a rubbery aspect. This rubbery state is also characterized by the existence of a glass transition temperature T_g, below which the polymer is solid and rigid (vitreous state), and above it, its stiffness modulus drops. It should be noted that the amorphous state has no melting temperature. The crystalline state is characterized by the regular configuration of molecular chains. This structure gives the polymer a rigid aspect. In this state, the melting temperature T_m exists and the material is much more rigid than in the amorphous state, because the crystalline structure is very compact.

After polymer melting, if the crystallization temperature is close to the melting value, the molecular chains have the freedom to move but the tendency to create a link is weak. As a result, the crystalline amount in the spherulite is very high while the growth is low. It should be noted that at macro-scale, the average crystalline amount is low because, at high temperature, the number of nucleations is low. When the temperature decreases, the molecular chains mobility decreases and the tendency to create a link increases, as a consequence the crystal amount in the spherulite decreases (Figure 1). The simulations observed in Figure 1, are carried out in thin film whose thickness equals 11 μm. Experimentally, it can be shown that there is no crystallization at a temperature above the melting temperature because the tendency to create a link between the molecules is nil. After melting, if the temperature drops very quickly to the glass transition temperature, the polymer chains do not have time to move and form crystals, as consequence the sample will be totally amorphous.

Crystallization can be modeled by the Kolmogorov model,[8] in order to calculate the probability (Poisson distribution) of existence of

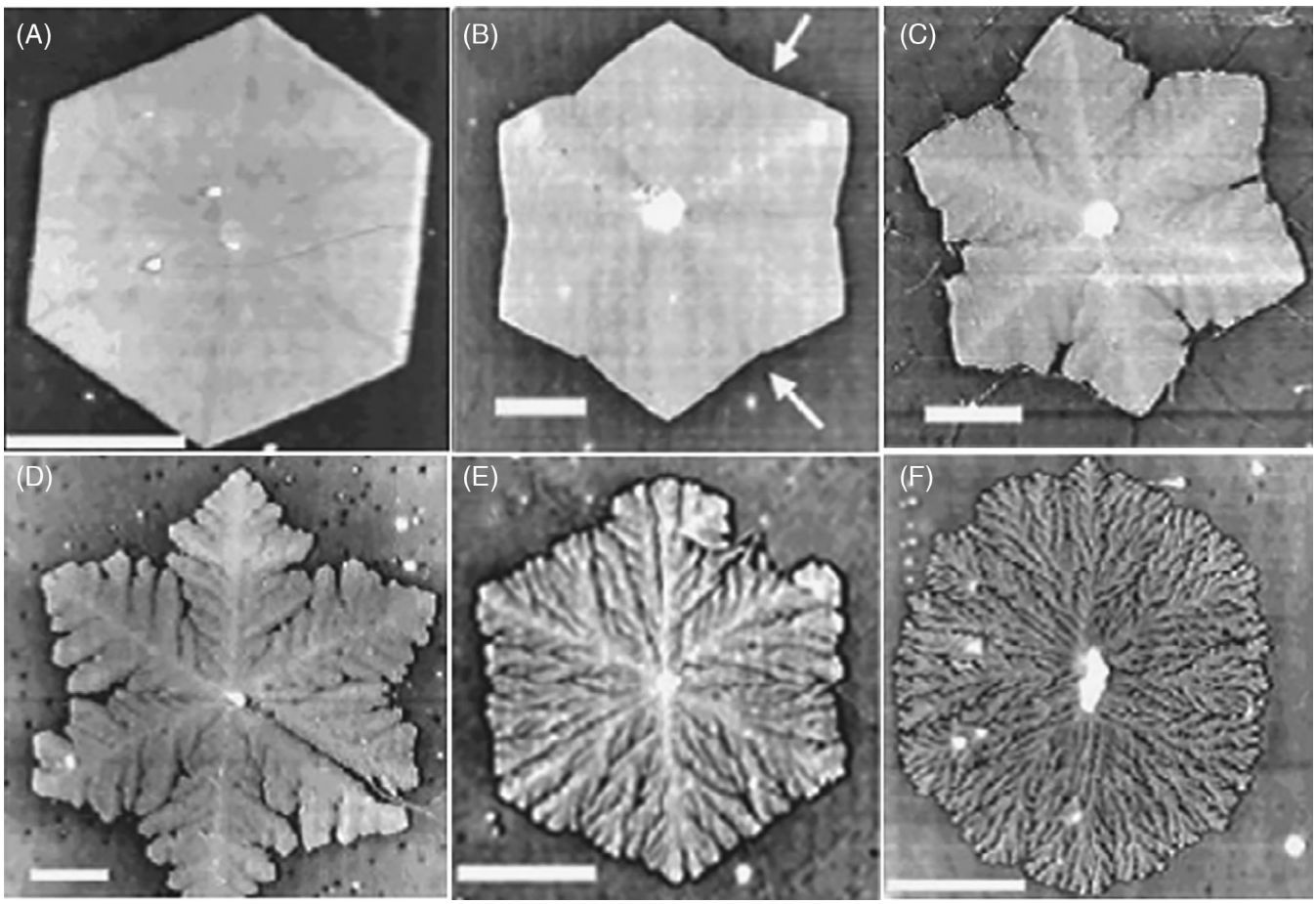

FIGURE 1 Experimental results[4] for isotactic polystyrene on the effect of crystallization temperature. (A) T_c = 210°C, 4 h, (B) T_c = 205°C, 4 h, (C) T_c = 200°C, 4 h, (D) T_c = 195°C, 3 h, (E) T_c = 190°C, 1 h, and (F) T_c = 180°C, 1 h. Scale bars are 5 μm

crystals as a function of nucleation and growth rate. In general, the temperature dependence of nucleation and growth rate should be evaluated separately. However, it is possible to establish a relationship between growth and nucleation by the isokinetic hypothesis, with the exception of polymers that crystallize very slowly. This is called the Nakamura model[9] which applies to noninsothermal cases. There is an extension to the isothermal case, assuming that nucleation and growth are constant during the process. This is called the Avrami model.[10] These two models can make a good approximation of the phenomenon, but they give only the normalized evolution of the degree of crystallization, that is, the evolution between the amorphous state, represented by (0), and the ultimate state of crystallization, represented by (1). Furthermore in multi-scale mechanical modeling, it is necessary to have access to the crystal amount in the structure, which is not possible with these models. To go further, a phase field model of crystallization has been developed, based on two equations, the Allen–Cahn Equation[11] which expresses the growth law and the heat transfer which expresses the temperature evolution. With this equation system, crystal growth evolution can be simulated. The nucleation can be modeled by a semianalytical model, it can be equal to a maximum number of nucleations multiplied by the nucleation probability, the probability is null at the melting temperature and maximum at the glass transition temperature.

Kobayashi[12] is one of the first who developed the phase field model, in order to show series of numerical simulations of the formation of various dendritic patterns, but his model gives qualitative results. His work is based on a representative model in nondimensional space and time. A serious concern with this model is that the evolution of crystal morphology as a function of temperature is not compatible with the physics of polymers. A few years later, Karma and Rappel[13] also used a nondimensional space and time phase field model. Their results are coherent with the exact prediction of the interface theory, but they did not test the temperature effect on the morphology and the crystallization degree for polymer. Xu et al.[14] make modifications to the phase field model essentially in the heat equation by changing the expression of the dimensionless heat of fusion, which weakens the basic theory of the phase field. Consequently, they obtain an evolution of the morphology consistent with the experimental test given by Taguchi,[7] but their simulation is not quantitative and the obtained simulation time is not correct. Hoffman-Lauritzen theory[15,16] shows that the spherulites growth is zero near the melting temperature T_m and that of the glass transition T_g. Except at T_m because it is considered as equilibrium temperature, the actual phase field model does not take into account the Hoffman–Lauritzen theory. Moreover, the crystal thickness is in the order of a few nm[17] especially when crystallization and melting temperatures are significantly apart. Therefore, for a quality numerical simulation, the micro structure's mesh or grid must be very fine. With available computer resources, it is not possible to do a simulation of a structure in mm by a mesh size in order of nm. In practice, the most used cell size is 0.1 μm, which allows to do simulation in large representative volume elements (RVEs). This value can satisfy simulations of very high temperatures close to T_m, but as soon as the temperature drops and the spherulite branches become very thin, the model loses its quantitative dimensional aspect. In addition, the phase field model requires that the temperature and the phase field variable evolve simultaneously. However, the polymer's heat diffusivity on the micoscopic scale gives an extremely rapid temperature evolution, whereas the phase evolution predicted by the equation is very weak. For this reason, most phase field models give very small times compared to the experimental observations. In conclusion, making fully quantitative predictions of crystal growth remains out of reach.

The objective of this work is to modify the phase field model in order to obtain experimentally consistent results according to the crystallization temperature evolution. To obtain quantitative simulations. We will target these characteristics: growth rate, crystal morphology and crystalline rate in the spherulite. The article has the following outline. In Section 2, there is a description of existing crystal growth models and the reasons that make them qualitative only. In Section 3, the phase field model is modified in order to make it consistent with polymer physics, as illustrated by 2D simulations. 3D simulations are presented in Section 4. Conclusions are drawn in Section 5. Mathematical proofs behind the phase field model are given in Appendix A.

2 | ORIGINAL PHASE FIELD MODELS

2.1 | Model description

Crystal evolution is controlled by two equations, the heat equation to control the temperature and check the equilibrium state (if the temperature equals the equilibrium value, there is no crystalline evolution) and the Allen–Cahn[11] equation which controls the crystalline phase evolution. In this equation system, there are two unknowns: a nonconserved phase field variable $\phi(X, t)$ and a temperature field $T(X, t)$ which both depend on space and time. ϕ is a nondimensional variable that varies between 0 and 1, with $\phi = 1$ meaning solid phase and $\phi = 0$ designating liquid or amorphous phase. These two equations are interrelated and this relationship creates the morphology of the crystal. The equation system is as follows, the proof is given in Appendix A.

$$\begin{cases} \dfrac{\partial \phi}{\partial t} &= -M\dfrac{\delta F(m(T),\phi)}{\delta \phi} \\ \dfrac{\partial T}{\partial t} &= \alpha \nabla^2 T + K\dfrac{\partial \phi}{\partial t} \end{cases} \tag{1}$$

Where M is a positive kinetic coefficient,[11] $1/M$ can also be defined as the characteristic time of attachment of atoms at the interface according to Karma,[13] F is the total free energy of the system, $\alpha = \frac{k_T}{\rho C_p}$ is the thermal diffusivity, $K = \frac{\Delta H}{C_p}$, ρ is the density, C_p is the specific heat at constant pressure, k_T is the thermal conductivity, ΔH is the latent heat, and $m(T)$ is a function that depends on temperature and will be given later.

The total free energy of the system of melt and solidifying crystals is defined as the Cahn–Hillard free energy.[18]

$$F(\phi,T)=\int_V f_{loc}dV=\int_V f_{liq-sol}(\phi,T)+f_{grad}(\phi)dV \quad (2)$$

With:

$$f_{liq-sol}(\phi,T)=W\int_0^{\phi}\phi(1-\phi)\left(\frac{1}{2}-\phi-m(T)\right)d\phi \quad (3)$$

$$f_{grad}(\phi)=\frac{1}{2}\epsilon^2(\nabla\phi)^2 \quad (4)$$

And

$$\frac{\delta F}{\delta\phi}=-\left[\nabla\cdot\left(\epsilon^2\nabla\phi\right)-\frac{\partial f_{loc}}{\partial\phi}\right] \quad (5)$$

The local free energy f_{loc} is divided into two parts, one describing the volume energy and the other, the interface energy. The volume part is considered as a double-well potential for Gibbs free energy containing two equilibrium points in the liquid state and in the crystalline one. Since the amorphous phase has none, the melting temperature of a semicrystalline material varies depending on the amount of crystalline phase. This property is added by changing T_m^0 by T_m in the crystal growth equation (see Appendix A), where T_m^0 is the equilibrium melting temperature and T_m is the melting temperature obtained at a specific crystallization temperature T_c. In order to add anisotropy to the crystalline form, the coefficient of interface energy gradient ϵ is taken not constant and is defined in 2D as follows.[13]

$$\epsilon=\bar{\epsilon}[1+\vartheta\cos(j(\theta-\theta_0))]\ \mid\ \theta=\arctan\left(\frac{\partial\phi/\partial y}{\partial\phi/\partial x}\right) \quad (6)$$

Where $\bar{\epsilon}$ is the reference interface energy gradient, ϑ is the strength of surface anisotropy, j is a form variable (when $j = 4$, the system represents a crystal structure with quadruple symmetry or when $j = 6$, the system represents a crystal structure which is sixfold symmetric), θ is the angle between the interface normal and the reference axis, and θ_0 is the spherulite orientation with respect to the horizontal axis, in this work $\theta_0 = 0$.

According to Kobayashi,[12] we can add some noise at the interface to get a different growth morphology for each direction, which is more realistic. The noise function is equal to $a\phi(1-\phi)R_v$ with $R_v \in [-1/2, 1/2]$ a random number.

As shown in Appendix A, Equation (1) can be rewritten under the following dimensionless form.

$$\begin{cases}\tau^*\hat{\epsilon}^2\dfrac{\partial\phi}{\partial\hat{t}} = \begin{bmatrix}\hat{\nabla}\cdot\left(\dfrac{1}{2}(\hat{\nabla}\phi)^2\dfrac{\partial\left(\hat{\epsilon}^2\right)}{\partial\hat{\nabla}\phi}\right)+\hat{\nabla}\cdot\left(\hat{\epsilon}^2\hat{\nabla}\phi\right)\\ -W\phi(\phi-1)\left(\phi-1/2+m\left(\hat{T}\right)\right)+a\phi(1-\phi)R_v\end{bmatrix}\\ \dfrac{\partial\hat{T}}{\partial\hat{t}} = \hat{\nabla}^2\hat{T}+\hat{K}\dfrac{\partial\phi}{\partial\hat{t}}\end{cases} \quad (7)$$

Where $\hat{T}=\frac{T-T_c}{T_m-T_c}$ is the dimensionless temperature, $\tau^*=\frac{\alpha}{\epsilon^2 M}$ is the dimensionless diffusivity, $\hat{K}=\frac{K}{T_m-T_c}$ is the dimensionless latent heat, $d\hat{t}=\frac{dt}{\tau}$ is the dimensionless time step, $\hat{\epsilon}=\frac{\epsilon}{D}$ is proportional to the dimensionless interface thickness, $d\hat{x}=\frac{dx}{D}$ is the dimensionless mesh size in X direction, $d\hat{y}=\frac{dy}{D}$ is the dimensionless mesh size in Y direction, and $d\hat{z}=\frac{dz}{D}$ is the dimensionless mesh size in Z direction. D and $\tau=\frac{D^2}{\alpha}$ are characteristic length and time, respectively. In this work $d\hat{x}=d\hat{y}=d\hat{z}=1$ and $d\hat{t}=0.1$. $d\hat{t}$ is defined so that the explicit resolution does not diverge. T_m in the dimensionless latent heat expression can be estimated by Hoffman Weeks theory[19]: $T_m=T_m^0\left(1-\frac{1}{2\beta}\right)+\frac{1}{2\beta}T_c$.

2.2 | Phase field model results and discussion

The resolution of the phase field model is based on the finite difference method. For efficiency, the implementation was done in C++ in a research version of the Digimat software.[20] The integration scheme is explicit with a stable time step computed according to the heat equation parameters. The numerical formulation is given in Appendix B.

The phase field model gives only the liquid–solid interface evolution, so it needs initial conditions. Since the simulations are performed at constant crystallization temperature T_c we consider that at time $t = 0$ there are N nucleations[21] which are circles in 2D and spheres in 3D placed in liquid at temperature T_c. Inside the nucleation, it is assumed that the temperature is equal to the equilibrium value and that the phase field parameter ϕ is equal to 1. While in the outside $\phi = 0$.

For now, we suppose 2D simulations, because the experimental observation (Figure 1) is made on a thin film. The model also works in 3D, but the anisotropy Expression (6) has to be adapted accordingly.

Polymers are well known for their low crystal growth rate, mostly at high temperatures (Figure 1), which gives a very low interface diffusivity. Theoretically, this phenomenon is controlled in the heat equation by $\hat{K}$ and in the growth equation by $m(T)$ which can be written in the dimensionless formulation as follows.

$$\begin{aligned}m\left(T_c,\hat{T}\right) &= \frac{\epsilon}{2k_{GT}}(T_m-T_c)\left(1-\hat{T}\right)\\ &= \frac{\epsilon}{2d_0\hat{K}}\left(1-\hat{T}\right)\end{aligned} \quad (8)$$

Where $d_0=k_{GT}\frac{C_p}{\Delta H}=\frac{\sigma T_m C_p}{\Delta H^2}$ is the capillary length and σ is the solid-liquid interface energy. At crystallization temperature near to that of fusion, $m\left(T_c,\hat{T}\right)$ becomes very weak, this means that the energy barrier of the double-well potential is waiting for its maximum and that the evolution of the interface has become difficult (Figure 2).

Kobayashi has simplified the expression of m and replaced it with an expression which does not show the effect of the crystallization temperature:

$$m\left(\hat{T}\right)=\frac{\alpha_k}{\pi}\arctan\left(\gamma_k\left(1-\hat{T}\right)\right) \quad (9)$$

where $\alpha_k = 0.9$ and $\gamma_k = 10^{12}$. Kobayashi shows that $m(T)$ should be such that $0 \le m(T) < 1/2$, because if $m(T) > 1/2$ the double-well potential appearance will be lost. In addition, we only work with $T < Tm$

because we are interested in simulating a solidification process, which implies $m(T) > 0$. In order to compare the effect of the modification of $m\left(T_c, \hat{T}\right)$, the parameters of the model will be fixed according to the nondimensional values given by Kobayashi.[12] To operate the model, the nondimensional parameter τ^* should be greater than or equal to 1, that is, thermal and phase field diffusivity must be close to each other. For example, Kobayashi used $\tau^* \hat{\epsilon}^2/(d\hat{x})^2 = 1/3$ and $\hat{\epsilon}/d\hat{x} = 1/3$ which gives: $\tau^* \hat{\epsilon}^2 = 0.0003$ for $d\hat{x} = 0.03$[12]. So, as we use $d\hat{x} = 1$, that gives $\hat{\epsilon} = 1/3$ and $\tau^* = 3$. Karma and Rappel[13] also used $\tau^* \in [1, 13]$.[13] Forcing phase field diffusivity to follow the thermal one causes incorrect simulation times, because physically the thermal diffusivity is very fast compared to the phase field one. To obtain a correct time, we can use the phase field diffusivity to calculate the characteristic time constant $\tau = \frac{D^2}{\epsilon M}$.

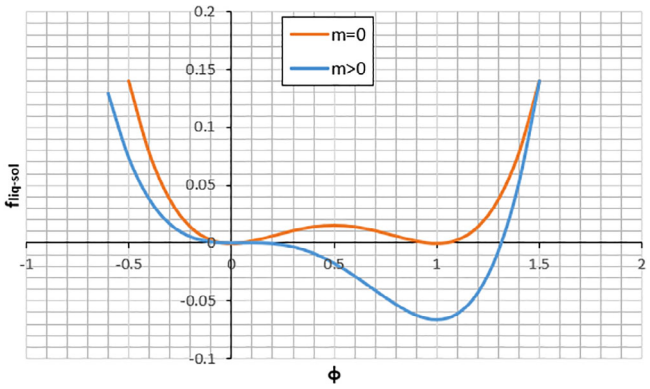

FIGURE 2 Effect of $m\left(T_c, \hat{T}\right)$ on the double-well potential $f_{\text{liq}-\text{sol}}$ Equation (3)

For all the following simulations, the yellow color represents the crystalline region, the black color between the crystalline branches represents the amorphous phase and the rest (outside the spherulite) represents the liquid phase. Figures 3 and 4 show the effect of the modification of $m\left(T_c, \hat{T}\right)$. Figure 3 represents Kobayashi model, comparing the results with those of experimental observation (Figure 1). It is clearly seen that when the temperature increases, the model predicts that the spherulites will have thinner branches and the crystal degree decreases, which is not physical. This problem will be fixed in Figure 4 thanks to the equation $m\left(T_c, \hat{T}\right) = \frac{\epsilon}{2d_0\hat{K}}\left(1 - \hat{T}\right)$. Unlike the Kobayashi model, there is a tendency to spread the crystalline branches as in the experimental observation of Figure 1, but with difficulty. If $\hat{K}$ tends to 0, spherulite growth "explodes" (Figure 5) and the growth continues without creating a crystal branch.

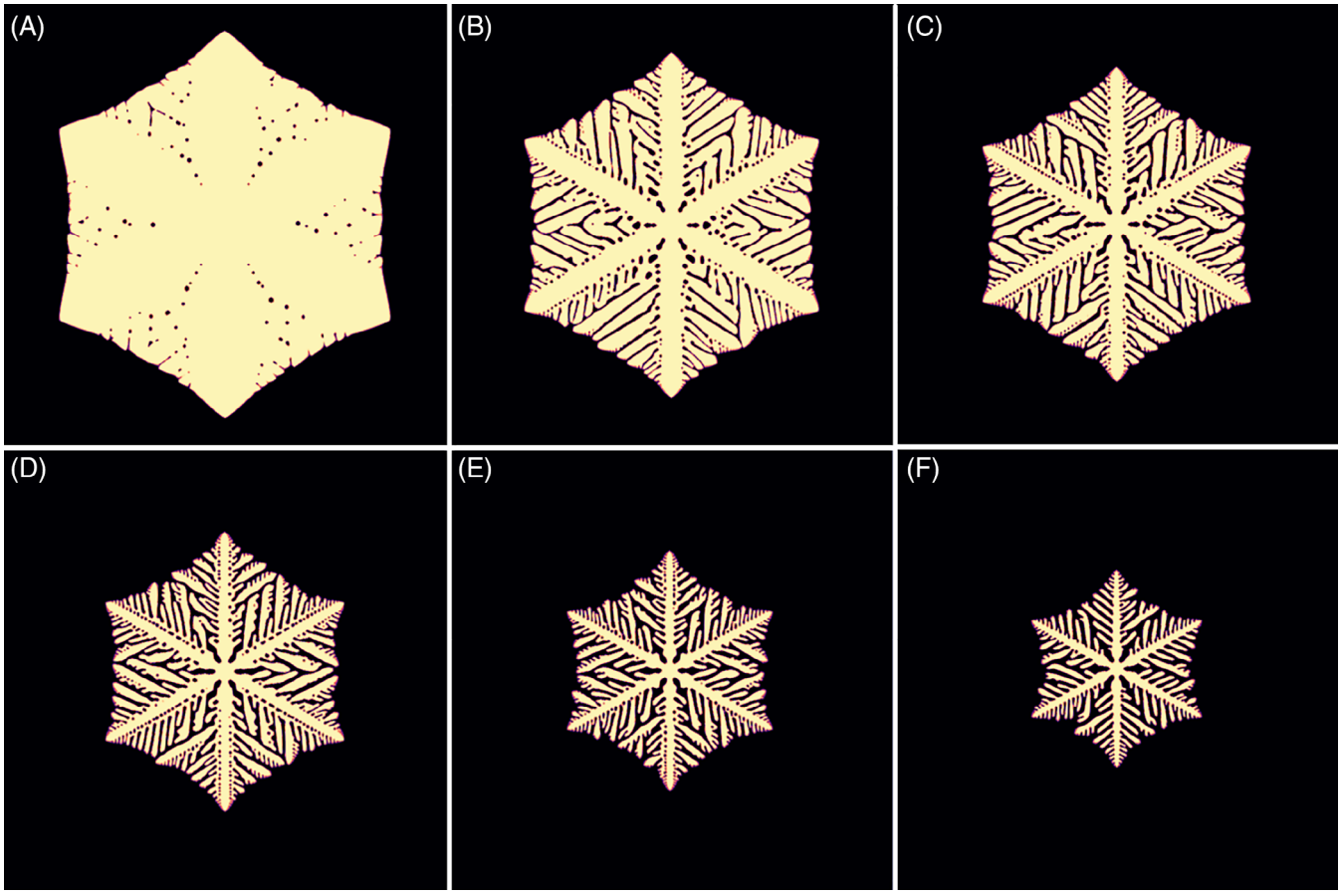

FIGURE 3 Predictions with Kobayashi's model[12] for isotactic polystyrene using $m\left(\hat{T}\right) = \alpha_k/\pi \arctan\left(\gamma_k\left(1 - \hat{T}\right)\right)$ and $K = 48.4°K$[14]: (A) $T_c = 180°C \Leftrightarrow \hat{K} = 1.08$, (B) $T_c = 190°C \Leftrightarrow \hat{K} = 1.28$, (C) $T_c = 195°C \Leftrightarrow \hat{K} = 1.42$, (D) $T_c = 200°C \Leftrightarrow \hat{K} = 1.59$, (E) $T_c = 205°C \Leftrightarrow \hat{K} = 1.81$ and (F) $T_c = 210°C \Leftrightarrow \hat{K} = 2.09$. Model parameters in Table 1, only $W = 1$. Grid Size 1000 X 1000 *Pixel*^{2}

Experimentally, when the glass transition temperature is approached, the spherulite size and the crystallinity degree will be small simultaneously. It can therefore be seen that the phase field model can be quantitative only near the melting temperature.

Xu et al.[14,22] tried to improve the phase field model for polymers, mainly by changing the expression of the dimensionless latent heat $\hat{K}$ taken as $\hat{K} = K/T_m$, where T_m is obtained by Hoffman Weeks expression. This modifies the dependence of $\hat{K}$ as a function of the crystallization temperature T_c. The model thus loses a theoretical basis and

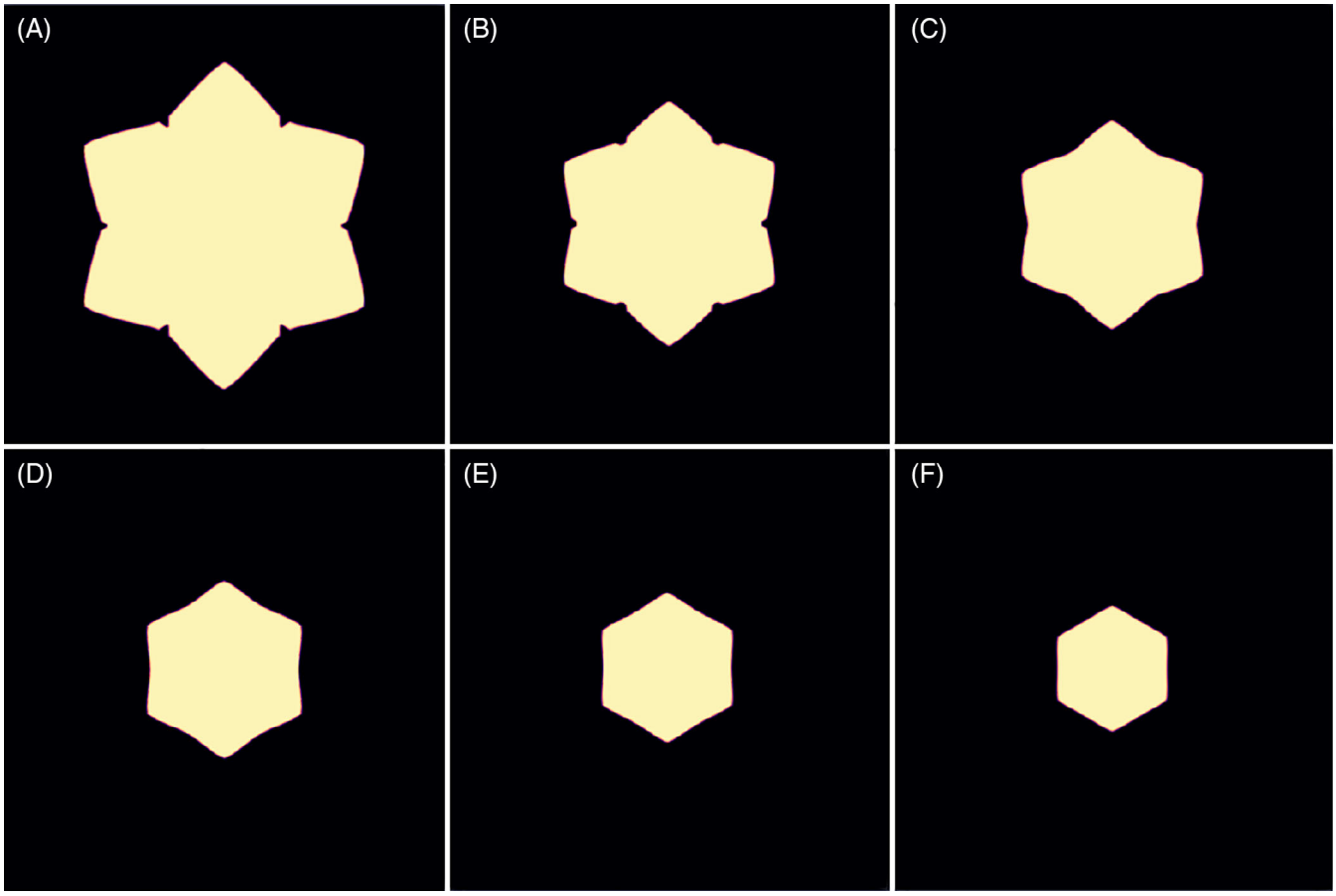

FIGURE 4 Predictions with Cahn-Allen model[11] for isotactic polystyrene using $m\left(T_c,\hat{T}\right) = \frac{\epsilon}{2d_0\hat{K}}\left(1-\hat{T}\right)$ and K = 48.4°K[14]: (A) T_c = 180°C $\Leftrightarrow \hat{K}$ = 1.08, (B) T_c = 190°C $\Leftrightarrow \hat{K}$ = 1.28, (C) T_c = 195°C $\Leftrightarrow \hat{K}$ = 1.42, (D) T_c = 200°C $\Leftrightarrow \hat{K}$ = 1.59, (E) T_c = 205°C $\Leftrightarrow \hat{K}$ = 1.81, and (F) T_c = 210°C $\Leftrightarrow \hat{K}$ = 2.09. Model parameters in Table 1, only W = 1. Grid size 500 X 500 *Pixel*^{2}

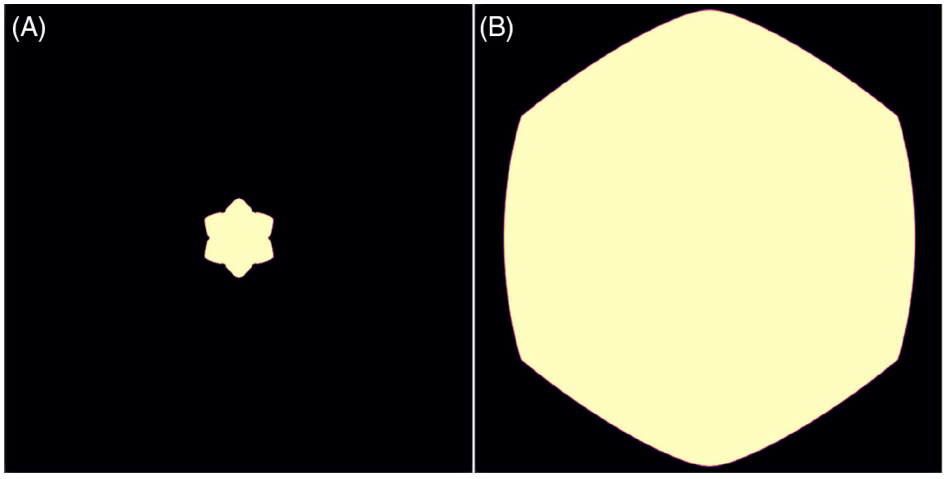

FIGURE 5 Predictions with Allen-Cahn model[11]: (A) $\hat{K}$ = 1.0, (B) $\hat{K}$ = 0.5. Model parameters in Table 1, only W = 1. Grid size 500 X 500 *Pixel*^{2}

the obtained simulations are not quantitative. Indeed, the time in the obtained simulations[14] for ITPS does not correspond to that of the experimental observation of Figure 1. The morphology evolution remained coherent but in a nonquantitative way.

3 | AN ENHANCED PHASE FIELD MODEL

In the phase field model, if we take all parameters as constant and vary the nondimensional parameter $\hat{K}$ (as in Kobayashi model, 3), the spherulite will have a small size and a low degree of crystallinity when $\hat{K}$ increases. Experimentally, this phenomenon can be observed between the maximum growth temperature $T_{c\ max}$ and the glass transition temperature T_g. But if we vary the dimensionless diffusivity $\tau^* = \frac{\alpha}{c^2 M}$, the spherulite will have a small size and a high degree of crystallinity when τ^* increases. Experimentally, this phenomenon can be observed between $T_{c\ max}$ and melting temperature T_m (Figure 1). In the proposed enhanced phase field model, we use the Kobayashi function $m(T)$ of eq. (9), but we give semi-analytical temperature-dependent expressions for parameters $\hat{K}$ and τ^* in order to correctly simulate the observed crystal growth phenomena.

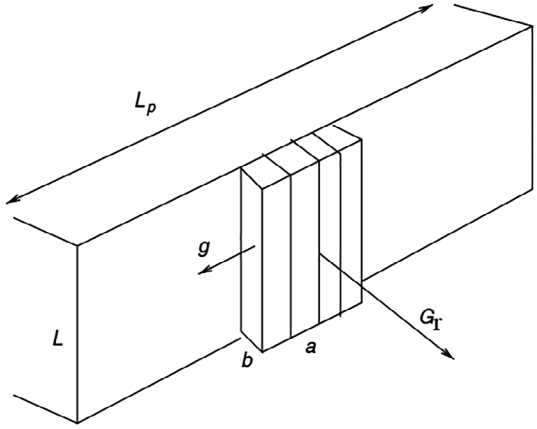

FIGURE 6 Lauritzen and Hoffman model of growth front[3]

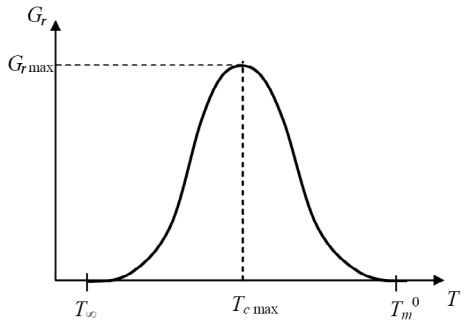

FIGURE 7 Crystalline growth rate according to the theory of Lauritzen and Hoffman: Equation (10)

3.1 | Semianalytical expression for the dimensionless diffusivity τ^* between $T_{c\ max}$ and T_m

Lauritzen and Hoffman (LH)[16] proposed a model for crystal growth as a function of temperature. In the basic LH model, the first nucleation is associated with the creation of the first growth surface, where L_p is its lateral dimension. While the second nucleation is the addition of the polymer molecules to the growing front, which is considered as stem, where $V = Lab$ is its volume, see sketch in Figure 6.

There are two ways to attach the stems to the growth front. The first is to put the stem at the growth surface in the direction of growth rate G_r. The second is to add a stem in the direction of lateral rate g (Figure 6). As a consequence, the stem formation is divided into three regimes:

- Regime I: if $g > > G_r$.

All the substrate is covered with stems before adding stem in the growth direction. This regime exists essentially at high temperature. This explains the fact that there is a high crystalline amount in spherulite at high temperature.

- Regime II: if $g = G_r$.

Stem growth occurs simultaneously in both directions. This regime occurs in medium temperature.

- Regime III: if $g < < G_r$.

The growth of the stem occurs essentially by deposition of new germs in the growth direction. This regime is obtained at low temperature.

The growth rate is proportional to two terms. The first corresponds to diffusion (or transport) of the macro-molecular chains in the liquid and the second to the deposit of germs on the surface of stem growth. Its expression given by LH theory is as follows.[15,16]

$$G_r(T_c) = G_{ri} \underbrace{\exp\left[-\frac{U^*}{k(T_c - T_\infty)}\right]}_{\text{Diffusion term}} \underbrace{\exp\left[-\frac{K_{G_r}}{T_c \Delta T}\right]}_{\text{Germ deposit}} \quad (10)$$

With: $G_{r\,i}$ is the prefactor for each regime $i \mid i \in$ [I, II, III] and:

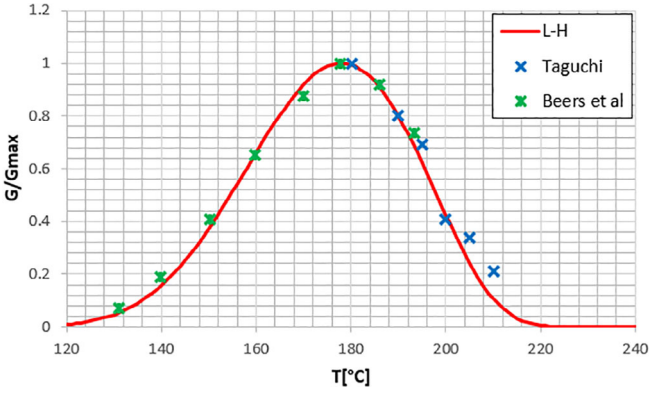

FIGURE 8 Calibration of the L-H function $\mathcal{H}(T_c)$, Equation 14. Experimental results given by refs. [7, 23]

$$K_{G_r} = \begin{cases} 2K_{G_{r0}} & \text{in regimes I \& III} \\ K_{G_{r0}} & \text{in regime II} \end{cases} \Big| K_{G_{r0}} = \frac{2b\sigma_l\sigma_f T_m^0}{k\Delta H} \quad (11)$$

where U^* is the activation energy for transport of segments to the site of crystallization, k is Boltzmann's constant, $T_\infty < T_g$ is the temperature at which any motion is made impossible, its expression is $T_\infty = T_g - 30°C$,[16] $\Delta T = T_m^0 - T_c$ is the super-cooling and σ_l and σ_f are the free energies of the lateral and frontal surfaces of the stem, respectively.

TABLE 1 Model parameters for isotactic polystyrene ITPS

Model parameters	Value	Model parameters	Value
$T_{c\,max}$	180°C[7,23]	$\Delta\hat{x}$	1.0
T_m^0	242°C[7]	$\frac{\varepsilon}{d_0}$	1.0
T_g	90°C[7]	β	1.5[14]
$\hat{\varepsilon}$	0.333[12]	τ_0^*	3.0[12]
$\Delta\hat{t}$	0.1	ϑ_0	0.06[14]
$\hat{K}_0$	1.4	a	0.02
j	6	W	2[24]
α_k	0.9[9]	γ_k	10^{12}

Since the phase field variation $\frac{\partial\phi}{\partial t}$ is proportional to the speed of propagation of the interface, then the evolution of $\frac{\partial\phi}{\partial t}$ and G_r must be similar. The idea is to combine the Cahn–Allen equation with the growth equation developed by LH. In this context, we modify the expression of the dimensionless diffusivity τ^*.

$$\tau^*(T_c) = \tau_0^*/\mathcal{H}(T_c) \quad (12)$$

where $\tau_0^* = \tau^*(T_{c\,max})$ is the reference dimensionless diffusivity, The expression of $\mathcal{H}(T_c)$ is obtained by Equation (9) as follows:

$$\mathcal{H}(T_c) = G_r(T_c)/G_r(T_{c\,max}) \quad (13)$$

Since we modify the expression of τ^* only between $T_{c\,max}$ and T_m, it corresponds theoretically to regime I. For simplicity, the following expression will be used.

$$\mathcal{H}(T_c) = h_0 \exp\left[-\frac{h_1}{T_c - T_\infty}\right] \exp\left[-\frac{h_2}{T_m^0 - T_c}\right] \quad (14)$$

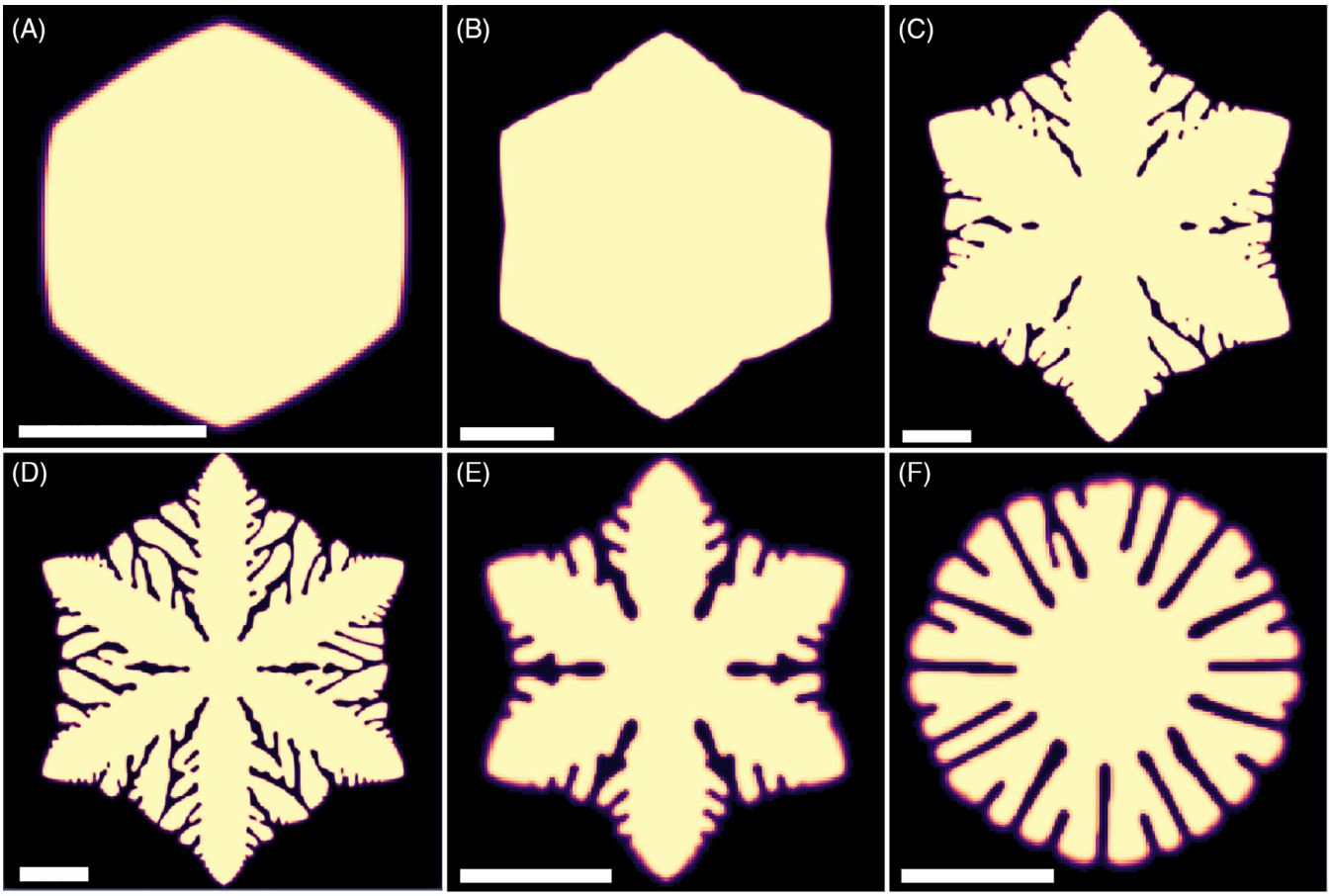

FIGURE 9 Simulation of changing the temperature effect for isotactic polystyrene with the proposed model of Equation (19). Mesh size $D = 10^{-7}$m. (A) $T_c = 210°C$, 4 h, (B) $T_c = 205°C$, 4 h, (C) $T_c = 200°C$, 4 h, (D) $T_c = 195°C$, 3 h, (E) $T_c = 190°C$, 1 h, and (F) $T_c = 180°C$, 1 h. Scale bars are 5 μm. Model parameters in Table 1

Where h_1 and h_2 are parameters and h_0 is obtained such that $\mathcal{H}(T_{c\,mac}) = 1$ and $\frac{d\mathcal{H}}{dT_c}(T_c = T_{c\,mac}) = 0$.

$$h_0 = \exp\left[\frac{h_1 + h_2 + 2\sqrt{h_1 h_2}}{T_m^0 - T_\infty}\right] \tag{15}$$

As a result, the simplified LH expression gives a bell-shaped curve. Figure 7 shows that the crystal growth evolution.

As we see in Figure 7, the crystal growth evolution as a function of temperature is consistent with the experimental result, that is, the growth rate is nonzero only between T_m^0 and T_∞ and there is no evolution outside this temperature range.

We assume that the model parameters will be calibrated at $T_{ref} = T_{c\ max}$ and the temperature dependence is taken only by $\mathcal{H}(T_c)$, so, $\hat{K}$ becomes a constant as a function of temperature and is calibrated at the reference temperature $T_c = T_{ref}$ ($\hat{K}$ is fixed, since its variation can change the growth rate).

Figure 1 shows that the anisotropy changes with temperature. In the model, in order to have a continuous function, we express the surface anisotropy strength as follows.

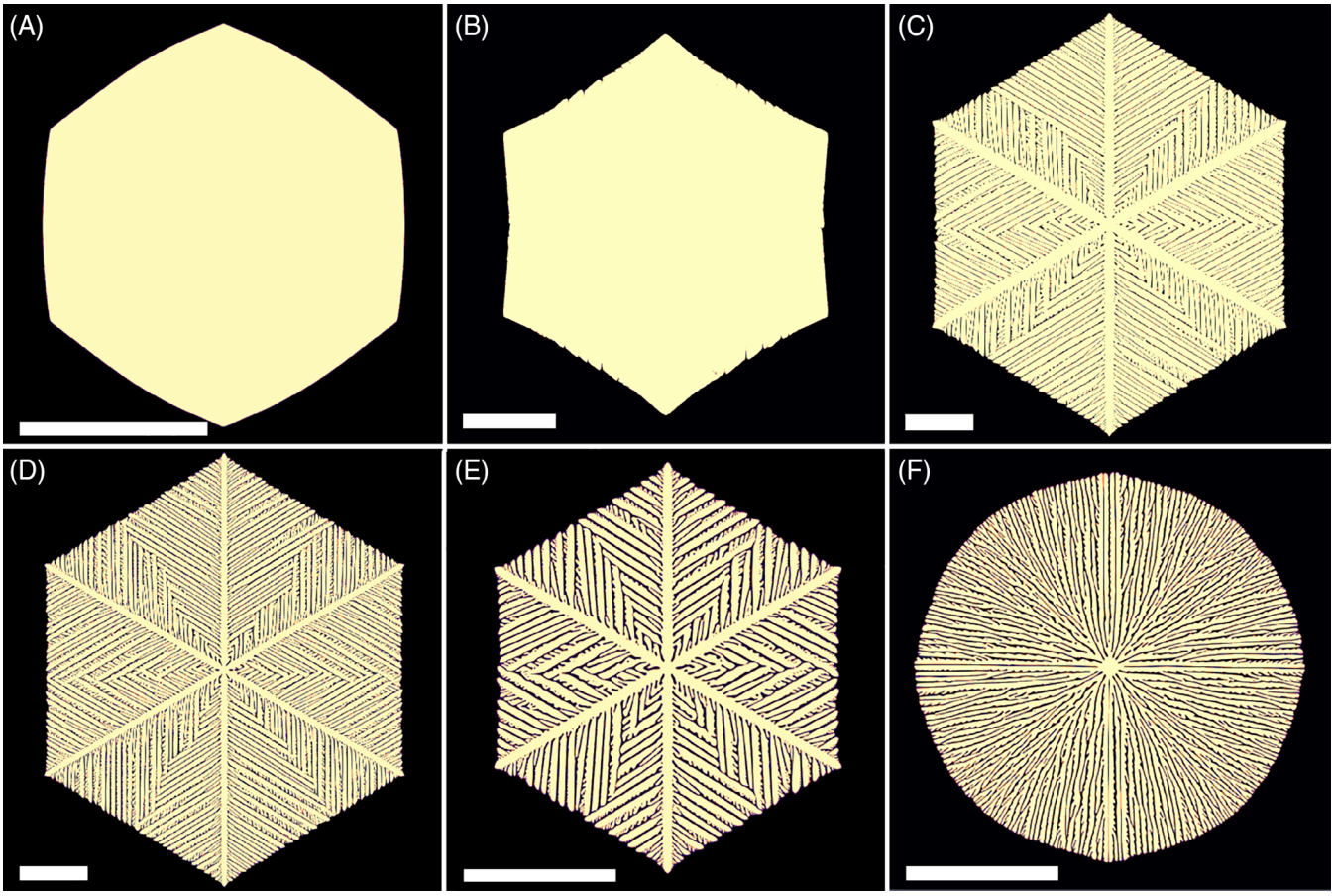

FIGURE 10 Simulation of changing the temperature effect for isotactic polystyrene with the proposed model of Equation (19). Mesh size $D = 10^{-8}$m. (A) $T_c = 210$°C, 4 h, (B) $T_c = 205$°C, 4 h, (C) $T_c = 200$°C, 4 h, (D) $T_c = 195$°C, 3 h, (E) $T_c = 190$°C, 1 h and (F) $T_c = 180$°C, 1 h. Scale bars are 5 μm. Model parameters in Table 1

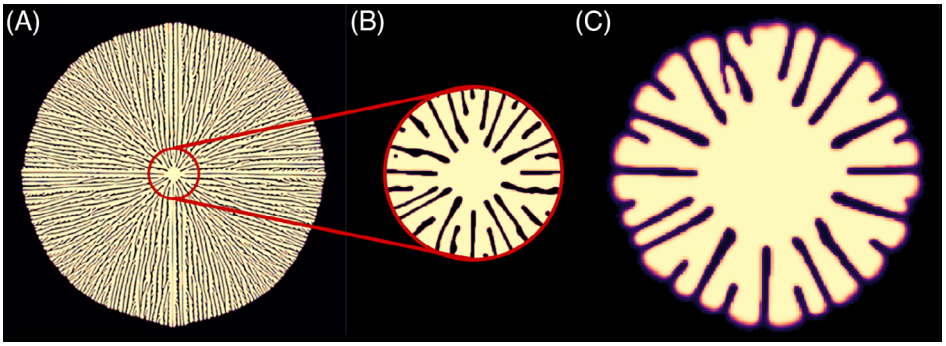

FIGURE 11 Simulations with the proposed model for $T_c = 180$°C. (A) crystal simulation with $D = 10^{-8}$m, (B) zoom on the crystal with $D = 10^{-8}$m, and (C) crystal simulation with $D = 10^{-7}$m

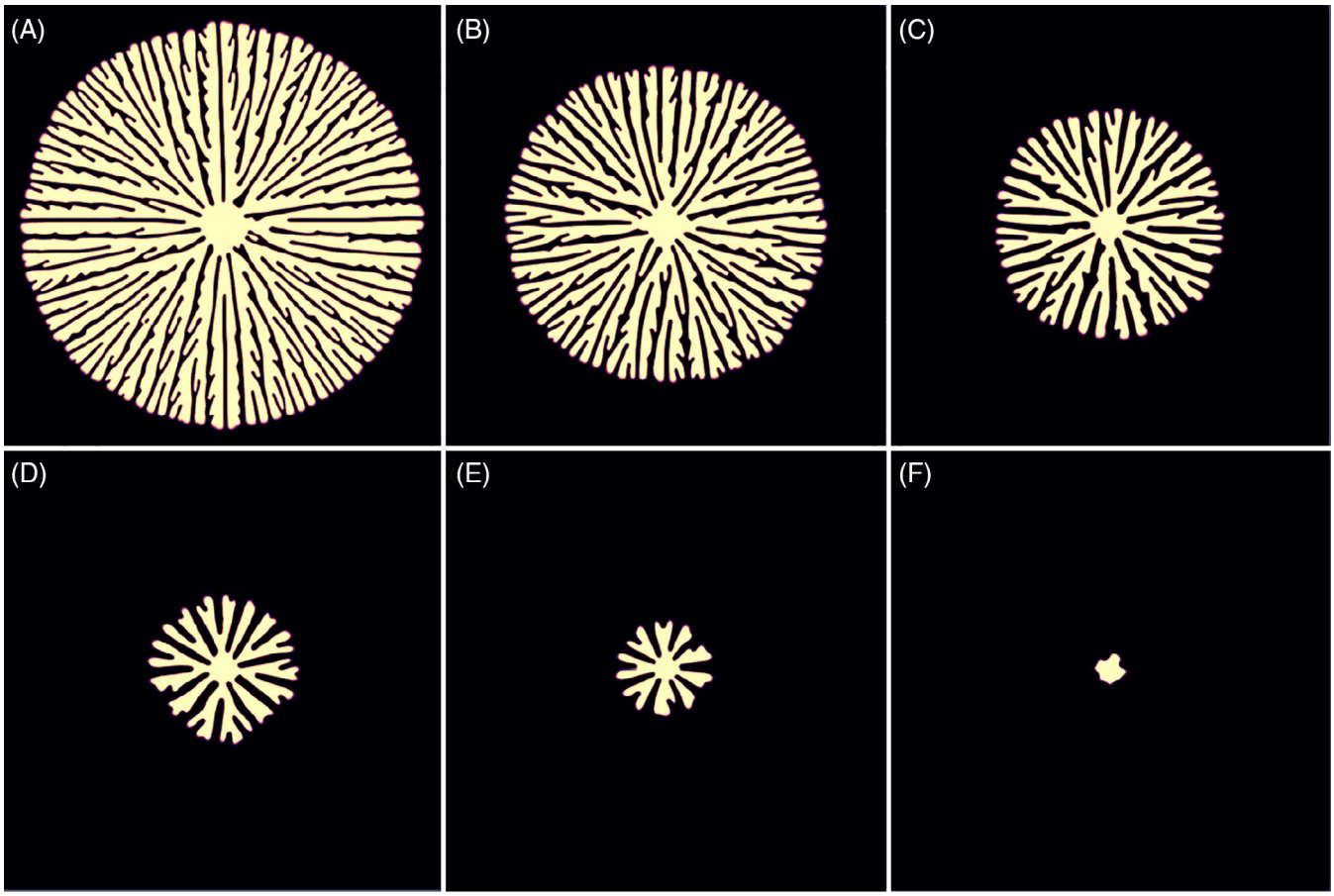

FIGURE 12 Simulations with the proposed model at time t = 4 h and film thickness 11 nm (A) T_c = 170°C, (B) T_c = 165°C, (C) T_c = 160°C, (D) T_c = 155°C, (E) T_c = 150°C, and (F) T_c = 140°C. Grid size 500 × 500 Pixel^2. (50 × 50 (μm)^2)

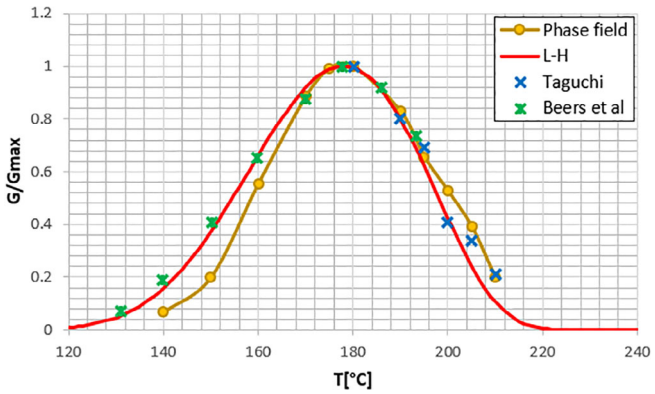

FIGURE 13 Spherulite growth given by phase field model compared to the L–H function $\mathcal{H}(T_c)$ (Equation 14) and the experimental result given by refs. [7, 23]

$$\vartheta(T_c) = \vartheta_0\left(\frac{\frac{2}{\pi}\arctan(\varpi(T_c - T_{crit})) + 1}{2}\right) \tag{16}$$

Where ϑ_0 is the reference strength of surface anisotropy. Assume that the anisotropy begins to disappear at $T_c = T_d$ and that there is no anisotropy after $T_c = T_f$, so ϖ calibrates the extension of the temperature domain $[T_d, T_f]$ and $T_{crit} = (T_d + T_f)/2$ is the critical temperature of change of anisotropy.

3.2 | Semianalytical expression for the dimensionless variable $\hat{K}$ between $T_{c\,max}$ and T_∞

Since we do not have a consistency with polymer physics at a temperature between the maximum growth temperature and the glass transition temperature, the model needs another correction. If we look at the behavior of the model, we can see that when we increase the nondimensional variable $\hat{K}$ in the heat equation, the spherulite size decreases and the crystal amount also decreases (Figure 4). In order to take advantage of this property, we take $\hat{K} \propto 1/\mathcal{H}(T_c)$. In this work we use the following function:

$$\hat{K}(T_c) = \begin{cases} \dfrac{\hat{K}_0}{\mathcal{H}(T_c)} & T_g \le T_c \le T_{c\,max} \\ \hat{K}_0 & T_{c\,max} < T_c \le T_m^0 \end{cases} \tag{17}$$

Where $\hat{K}_0$ is calibrated at $T_c = T_{c\ max}$ (temperature of maximum growth rate).

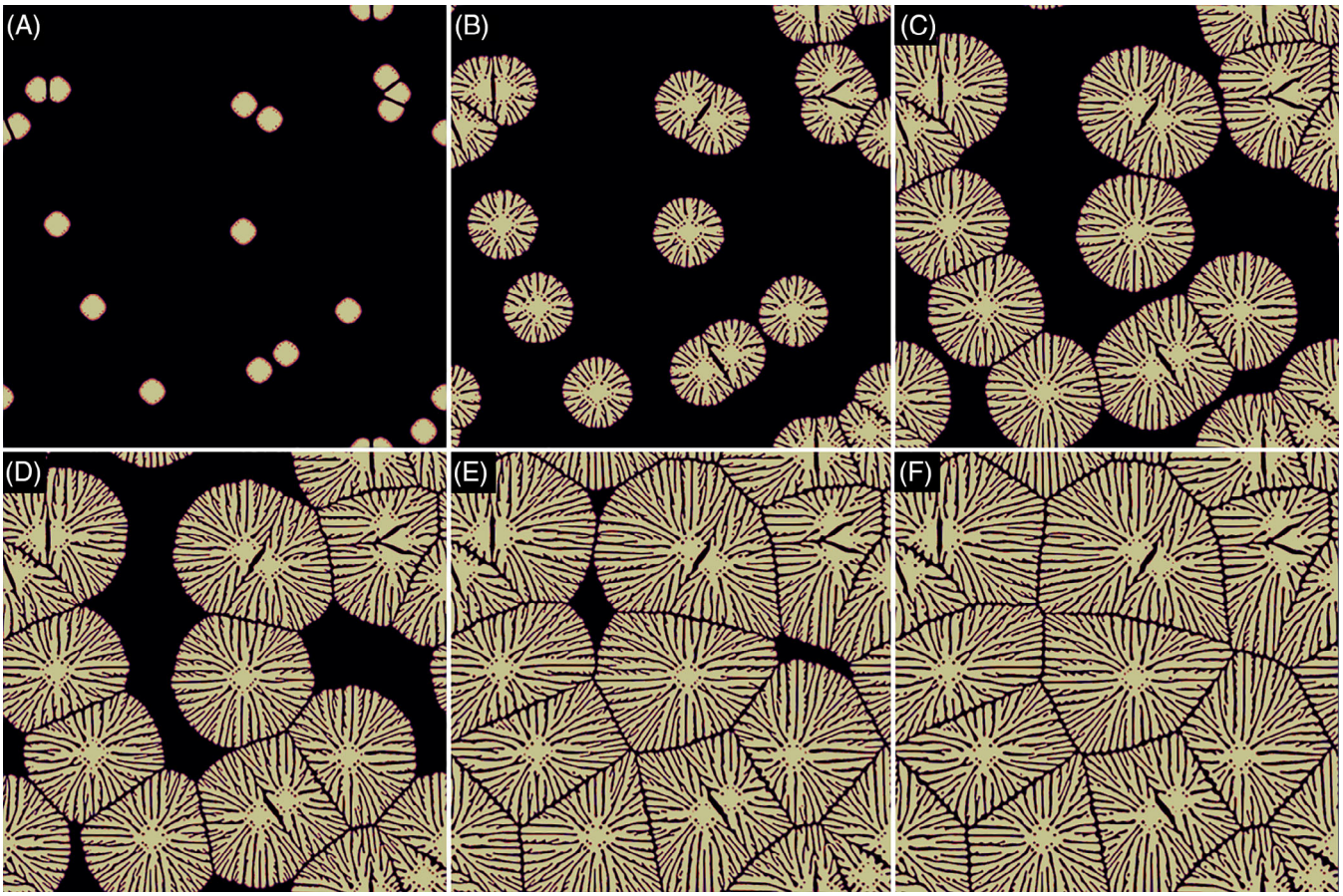

FIGURE 14 Simulation with the proposed model of isotactic polystyrene crystallization at T_c = 169°C, (A) t = 26 min, (B) t = 1 h 18 min, (C) t = 2 h 10 min, (D) t = 2 h 36 min, (E) t = 3 h 28 min, and (F) t = 4 h 20 min. Grid size 1500 × 1500 Pixel^2, (150 × 150 (μm)^2), Table 1

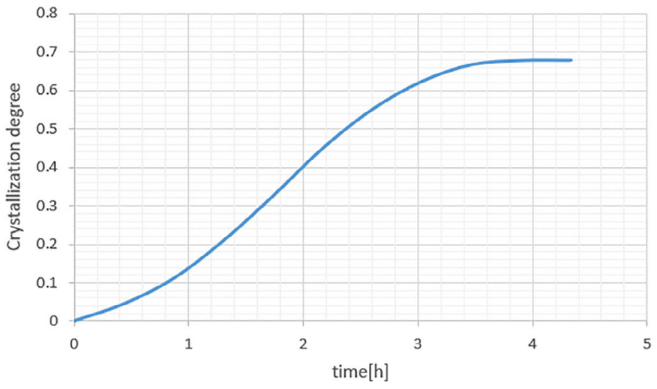

FIGURE 15 Simulation with the proposed model of crystallization degree as a function of time, in 2D for isotactic polystyrene at T_c = 169°C (data in Table 1)

$$\tau^*(T_c) = \begin{cases} \dfrac{\tau_0^*}{\mathcal{H}(T_c)} & T_{c\,max} < T_c \le T_m^0 \\ \tau_0^* & T_g \le T_c \le T_{c\,max} \end{cases} \tag{18}$$

After modification, the model Equations (7) become:

$$\begin{cases} \tau^*(T_c)\hat{\epsilon}^2\dfrac{\partial\phi}{\partial\hat{t}} = \begin{bmatrix} \hat{\nabla}\cdot\left(\dfrac{1}{2}\left(\hat{\nabla}\phi\right)^2\dfrac{\partial\left(\hat{\epsilon}^2\right)}{\partial\hat{\nabla}\phi}\right) + \hat{\nabla}\cdot\left(\hat{\epsilon}^2\hat{\nabla}\phi\right) \\ -W\phi(\phi-1)\left(\phi-1/2+m\left(\hat{T}\right)\right) + a\phi(1-\phi)R_v \end{bmatrix} \\ \dfrac{\partial\hat{T}}{\partial\hat{t}} = \hat{\nabla}^2\hat{T} + \hat{K}(T_c)\dfrac{\partial\phi}{\partial\hat{t}} \end{cases} \tag{19}$$

It should be noted that $\tau^*(T_c)$ must be equal to τ_0^* at a temperature between the maximum growth temperature and the glass transition temperature and it takes the value of Equation (12) at a temperature between the maximum growth temperature and the equilibrium melting temperature.

3.3 | Results and discussion

Between temperatures $T_{c\,max}$ and T_m, the model calibration is done in two steps, the first consists in calibrating the function $\mathcal{H}(T_c)$. Figure 8 represents the fit of the function $\mathcal{H}(T_c)$ with the experimental data,

which are given by Taguchi et al.[7] and Kathryn L. Beers et al.[23] The second step is to calibrate $\hat{K}_0$ at the maximum growth temperature which is taken equal to 180°C which controls the crystalline degree, the other parameters of the phase field model are taken according to Kobayashi[12] (Table 1). Among the non-dimensional parameters of the model, the only parameter which depends on the characteristic length D is $\hat{\varepsilon} = \varepsilon/D$. So, the variation of D will affect the numerical stability through $\hat{\varepsilon}$. The idea in this work is therefore to fix $\hat{\varepsilon}$ to ensure numerical stability, and the characteristic length D is fixed by comparing experimental observations with model predictions. This method introduces a mesh dependency (figures 9 and 10). However, the characteristic length D must be less than the interface thickness 6ε to ensure numerical stability: $D \leq 6\varepsilon$. This gives: $\hat{\varepsilon} \geq \frac{1}{6}$.

Figure 9 shows the evolution of the crystal morphology according to temperature, now we can see that there is a consistency with experimental observations. The use of a large space step can give good results at high temperature, but as soon as the temperature drops, the crystal thickness will be low, the model cannot display correctly the size of the crystal thickness. If we reduce the mesh size (Figure 10), at high temperature, the crystal thickness becomes very small compared to the experimental observation. In addition, if we look at Figure 11 we can see that the crystalline amount in the spherulite does not change with the change of space step (we do not consider the primary nucleation circle, only the ratio between the crystalline branch and the amorphous branch interests us). Moreover, by using a coarser mesh, the simulation time will be faster, in this case, we can easily make simulations on a larger scale. For these reasons, we will avoid reducing the mesh size. An interesting feature about this method is that we can assign a suitable value to the characteristic length D without knowing the value of the interface thickness 6ε. There is indeed a mesh dependency, but the numerical stability is ensured.

Figure 12 shows the evolution of the crystal at temperatures below the maximum growth temperature $T_{c\ max}$. We can see that the result agrees with polymer physics.

According to the experimental results, the maximum growth is given at T_c = 180°C and is noted G_{max}. Figure 13 shows the comparison between phase field result, the L–H function $\mathcal{H}(T_c)$ and the experimental results given by Taguchi et al.[7] and Beers et al.[23] This comparison shows that the phase field model is predictive with a certain error, which is concentrated according to the figure between $T_{c\ max}$ and T_g. The phase field spherulite growth curve does not follow exactly the L–H curve (Equation 1) because the evolution of the phase field variation $\frac{\partial \phi}{\partial t}$ is not linear as a function of τ^* and $\hat{K}$.

3.4 | Virtual simulation of crystallization phenomena

When a polymer liquid is subjected to a temperature below its melting temperature, small nuclei of different sizes and shapes are born. This phenomenon can be called primary nucleation. These nuclei are stabilized when the free energy associated with the formation diminishes. So to simulate crystallization, we need a nucleation law.

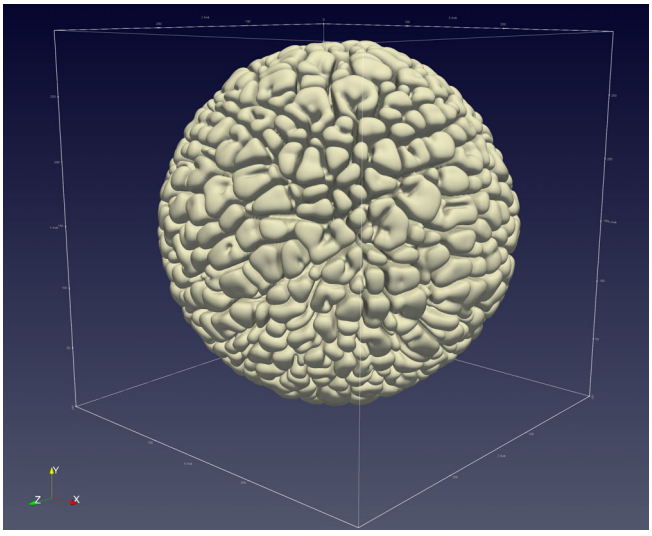

FIGURE 17 Simulation of 3D spherulite with the proposed model at T_c = 180°C. Grid size 300 × 300 × 300 Pixel^3, (30 × 30 × 30 (μm)^3)

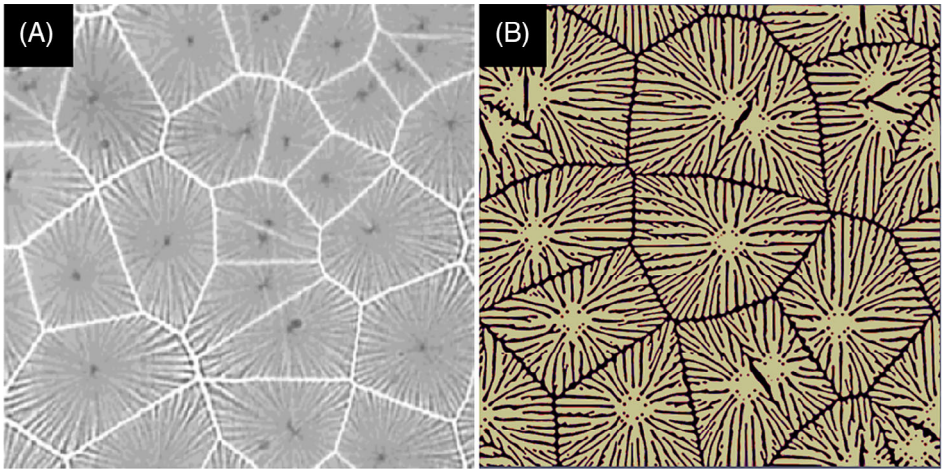

FIGURE 16 (A) Experimental observation at T_c = 169°C and film thickness equal to 60 nm,[23] (B) numerical simulation with the proposed model at T_c = 169°C and film thickness equal to 11 nm. (150 × 150 (μm)^2)

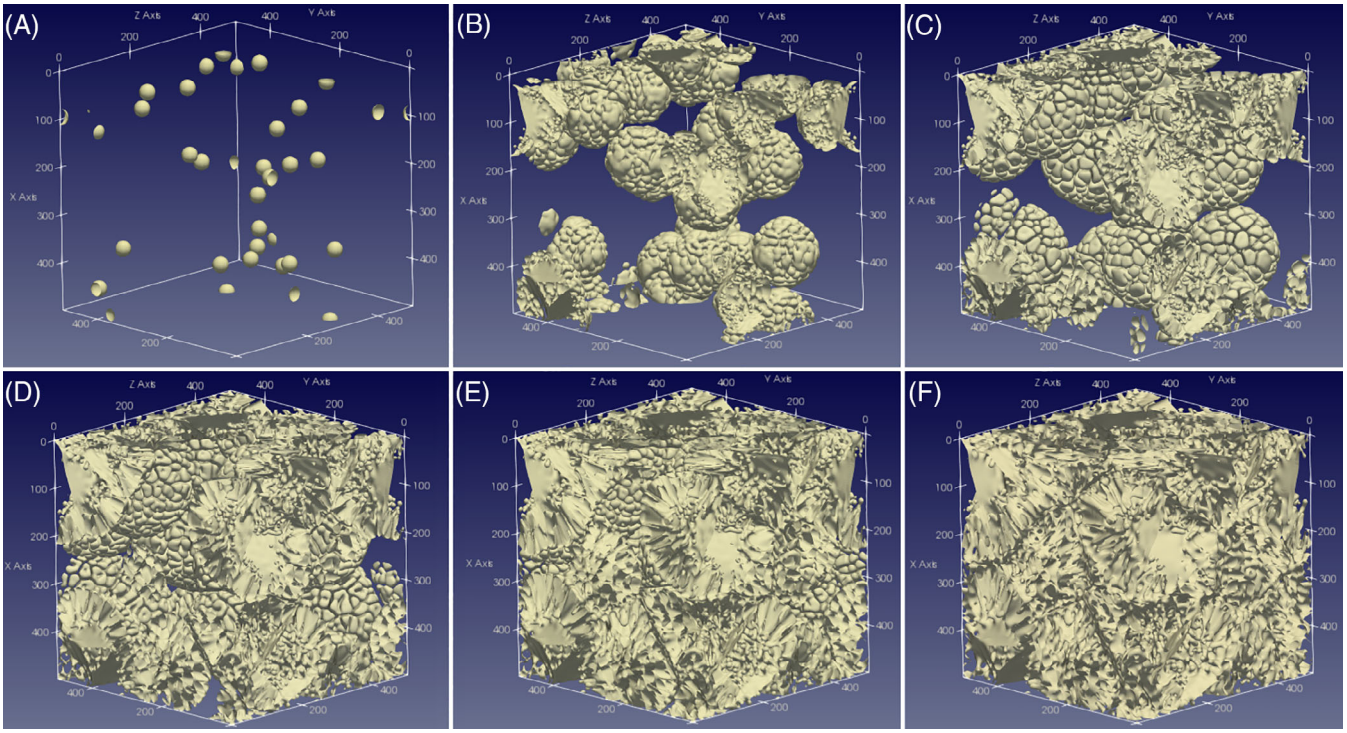

FIGURE 18 3D simulation with the proposed model of isotactic polystyrene crystallization at T_c = 169°C, (A) at time t = 10 min 30 s, (B) at time t = 1 h 5 min, (C) at time t = 1 h 24 min, (D) at time t = 1 h 45 min, (E) at time t = 2 h 6 min, and (F) at time t = 3 h 9 min. Grid size 500 × 500 × 500 Pixel^3, (50 × 50 × 50 (μm)^3). (evolution of the solid–liquid interface)

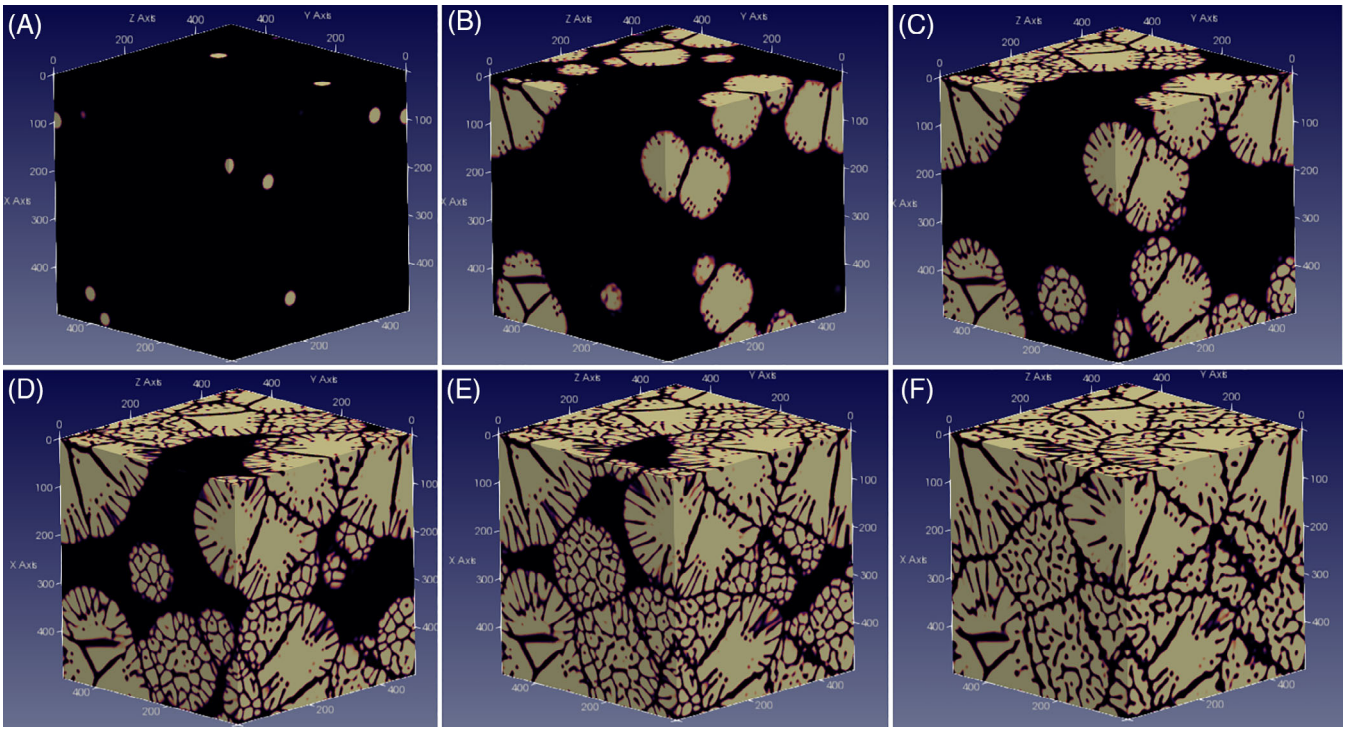

FIGURE 19 3D simulation with the proposed model of isotactic polystyrene crystallization at T_c = 169°C, (A) at time t = 10 min 30 s, (B) at time t = 1 h 5 min, (C) at time t = 1 h 24 min, (D) at time t = 1 h 45 min, (E) at time t = 2 h 6 min, (F) at time t = 3 h 9 min. Grid size 500 × 500 × 500 Pixel^3, (50 × 50 × 50 (μm)^3). (spherulite evolution in the liquid phase)

Since we do not have experimental data on the number of nucleations for a film thickness equal to 11 nm (the film is the sample used in the observation test), we will choose an approximate number at T_c = 169°C according to the experimental observation given by Beers.[23] The nucleation position is taken random.

Figure 14 shows the evolution of crystal growth from multi-nucleation at T_c = 169°C. By calculating the average of the phase field variable ϕ, we can plot the crystal amount curve as a function of time (Figure 15).

In Figure 16, there are two images of a simulation and an experimental observation. It should be noted that we cannot make a direct comparison between these two images because they do not have the same film thickness, but we can see that there is a consistency between the simulation and the experimental result.

4 | GENERALIZATION TO 3D SIMULATIONS

3D simulations are investigated by using Equations (19). It is assumed that the crystallization temperature is uniform in the structure and the interface energy gradient ε is taken constant. Figure 17 shows the morphology of a spherulite formed at temperature equal to 180°C.

Figures 18 and 19 show the crystal evolution simulation at temperature equal to 169°C and RVE size equal to $50 \times 50 \times 50$ $(\mu m)^3$. This 3D model does not take into account the film thickness change effect. For this reason, using thin-film polymer parameters makes this 3D representation qualitative. Indeed reducing the thickness of the film causes a difficulty for crystal propagation, because the film thickness will be comparable to that of the crystal (L in Figure 6). In addition, we used a large number of nucleations in a small RVE to reduce the simulation time, as a result the time scale in Figure 15 is different from that time scale in Figure 20, but we can see that the ultimate crystallization remains the same. It should be noted that the CPU time in the 2D simulation (Figure 14) is 15 times faster than the 3D one (Figure 18) on the same computer (16GB of RAM): 33 min in 2D and 8 h 25 min in 3D.

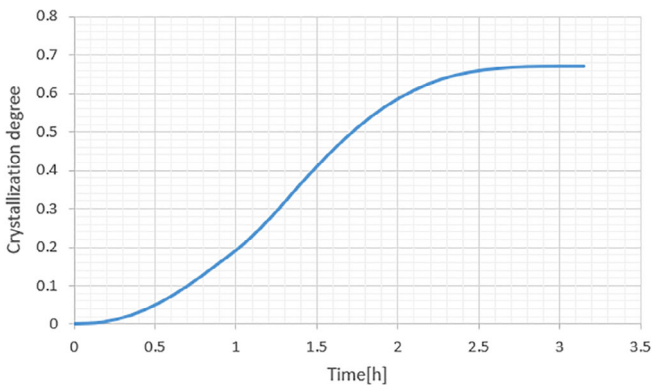

FIGURE 20 Simulation with the proposed model of crystallization degree as a function of time, in 3D for isotactic polystyrene at T_c = 169°C (data in Table 1)

5 | CONCLUSION

Crystallization can be defined as the solid-liquid interface evolution in time and space. One of the best-known models in the literature is the phase field model which controls the interface evolution using the Allen–Cahn equation of crystal growth and the heat transfer equation.

However, as shown in Section 2, the phase field model only gives a qualitative representation and can lead to nonphysical results. This is the case for the well-known Kobayashi model,[12] and also for the Xu et al. model,[14] where the modifications made to the phase field model do not render it quantitative. In this study, we tried to improve this model by adding two semianalytical expressions for the dimensionless diffusivity τ^* and $\hat{K}$, the dimensionless fraction between the latent heat of solidification and the specific heat at constant pressure. The dimensionless diffusivity τ^* and the expression of $\hat{K}$ are taken according to LH theory.[15] The proposed model in Section 3 is capable of quantitative prediction of growth, as shown in Figure 13. The given morphology is also close to experimental results (Figure 9), except those with temperature below 190°C. It has been shown that simulations do not become quantitative when the mesh size is too small. In some cases, the crystal branch becomes very thin compared to reality. As the change of mesh size does not modify the crystallinity degree in the spherulite, a coarse mesh was chosen which enables a significant gain in computation time.

Adding some approximations weakens the original phase field theoretical model, but helps to obtain results which are more consistent with polymer physics (Figures 9, 13, and 16). However, we cannot claim that the predictions are completely quantitative because the branch size is not respected for temperatures far from that of the fusion. In addition, the crystallization degree evolution is controlled proportionally with the growth rate by the functions $\tau^*(T_c)$ and $\hat{K}(T_c)$, but in reality each property can evolve independently.

Besides addressing the shortcomings of the current version of the proposed phase field model, the long term goal is to embed it within ICME (Integrated Computational Materials Engineering), bridging process simulation to structural engineering via crystallinity prediction and the way it influences the performance of semicrystalline polymers. In order to do so, the following extensions are needed:

- Coupling the model with homogenization techniques in order to predict the engineering properties based on spherulite morphologies.
- Linking the model with thermo-mechanical simulations at structural level in order to predict the spatial variability of crystallinity.

ACKNOWLEDGMENTS

This research was supported by Luxembourg national research fund FNR with collaboration between e-Xstream engineering sarl (part of Hexagon Manufacturing Intelligence) and Université catholique de Louvain. The research project acronym is SIMAMPO, and aims at modeling the SLS (Selective Laser Sintering) process for polymer applications.

ORCID

Issam Doghri https://orcid.org/0000-0001-8297-1297

REFERENCES

[1] H. Meijer, L. Govaert, *Mechanical Performance of Polymer Systems: The Relation Between Structure and Properties*, 30, Elsevier, **2005**, 915. https://doi.org/10.1016/j.progpolymsci.2005.06.009.
[2] M. C. Boyce, D. M. Parks, A. S. Argon, *Mech. Mater.* **1988**, *7*, 15. https://doi.org/10.1016/0167-6636(88)90003-8.
[3] M. Muthukumar, *Advances in Chemical Physics*, Vol. 128, Wiley, Massachusetts **2004**. https://doi.org/10.1002/0471484237.ch1.
[4] R. Spina, M. Spekowius, C. Hopmann, *Thermochimica Acta.* **2018**, *659*, 44 https://doi.org/10.1016/j.tca.2017.10.023.
[5] H. Yokota, T. Kawakatsu, *Polymer* **2020**, *186*, 121975 https://doi.org/10.1016/j.polymer.2019.121975.
[6] H. Yokota, T. Kawakatsu, *Polymer* **2017**, *129*, 189 https://doi.org/10.1016/j.polymer.2017.09.022.
[7] K. Taguchi, H. Miyaji, K. Izumi, A. Hoshino, Y. Miyamoto, R. Kokawa, *Polymer* **2001**, *42*, 7443. https://doi.org/10.1016/S0032-3861(01)00215-4.
[8] A. Kolmogorov, *Izvestia Akademii Nauk SSSR* **1937**, *1*, 355 https://www.bibsonomy.org/bibtex/224fd6d8e53caf97b0510736ae99e5e63/peter.ralph.
[9] K. Nakamura, T. Watanabe, K. Katayama, T. Amano, *J. Appl. Polym. Sci.* **1972**, *16*, 1077. https://doi.org/10.1002/app.1972.070160503.
[10] M. Avrami, *J. Chem. Phys.* **1939**, *7*, 1103. https://doi.org/10.1063/1.1750380.
[11] J. Cahn, S. Allen, *J. Phys. Colloq.* **1977**, *38*, C7 https://hal.archives-ouvertes.fr/jpa-00217210.
[12] R. Kobayashi, *Phys. D.* **1993**, *63*(1993), 410. https://doi.org/10.1016/0167-2789(93)90120-P.
[13] A. Karma, W.-J. Rappel, *Phys. Rev. E* **1998**, *57*, 4323. https://doi.org/10.1103/PhysRevE.57.4323.
[14] H. Xu, R. Matkar, T. Kyu, *Phys. Rev. E* **2005**, *72*, 011804. https://doi.org/10.1103/PhysRevE.72.011804.
[15] J. D. Hoffman, L. J. Frolen, G. S. Ross, J. I. Lauritzen, *J. Res. Nat. Bureau Stand-A. Phys. Chem.* **1972**, *79A*, 671. https://doi.org/10.6028/jres.079a.026.
[16] J. D. Hoffman, J. I. Lauritzen, *J. Res. Nat. Bureau Stand-A. Phys. Chem.* **1961**, *65A*, 297. https://doi.org/10.6028/jres.065A.035.
[17] A. Keller, M. Hikosaka, S. Rastogi, A. Toda, *Philos. Trans. Royal Soc. London* **1994**, *348*, 3. https://doi.org/10.1098/rsta.1994.0077.
[18] J. Cahn, J. Hilliard, *J. Chem. Phys.* **1958**, *28*, 258. https://doi.org/10.1063/1.1744102.
[19] J. D. Hoffman, J. Weeks, *J. Res. Nat. Bureau Stand-A. Phys. Chem.* **1962**, *66A*, 13. https://doi.org/10.6028/jres.066a.003.
[20] Digimat, the nonlinear multiscale material and process modeling platform, version 2019.1, October 2019, e-Xstream engineering part of Hexagon Manufacturing Intelligence.
[21] Y. Tong, Y. Lin, S. Wang, M. Song, *Int. J. Sci. Technol. Polymer* **2015**, *73*, 52. https://doi.org/10.1016/j.polymer.2015.07.025.
[22] H. Xu, W. Keawwattana, T. Kyu, *J. Chem. Phys.* **2005**, *123*, 124908. https://doi.org/10.1063/1.2036976.
[23] K. L. Beers, J. F. Douglas, E. J. Amis, A. Karim, *Langmuir* **2003**, *19*, 3935. https://doi.org/10.1021/la026751r.
[24] C. Beckermann, H. Diepers, I. Steinbach, A. Karma, X. Tong, *J. Comp. Phys.* **1999**, *154*(1999), 468. https://doi.org/10.1006/jcph.1999.6323.
[25] N. Valizadeh, T. Rabczuk, *Comp. Methods. Appl. Mech. Eng.* **2019**, *351*, 599. https://doi.org/10.1016/j.cma.2019.03.043.
[26] H. Gomez, V. M. Calo, Y. Bazilevs, T. J. R. Hughes, *Comp. Methods. Appl. Mech. Eng.* **2008**, *197*, 4333. https://doi.org/10.1016/j.cma.2008.05.003.
[27] R. Sanal, Numerical simulation of dendritic crystal growth using phase field method and investigating the effects of different physical parameter on the growth of the dendrite (**2014**). arXiv: 1412.3197.

How to cite this article: Bahloul A, Doghri I, Adam L. An enhanced phase field model for the numerical simulation of polymer crystallization. *Polymer Crystallization*. 2020;3: e10144. https://doi.org/10.1002/pcr2.10144

APPENDIX A: PROOF OF CRYSTAL GROWTH AND HEAT EQUATION

Crystal growth equation

The phase field equation is given by the Gibbs–Thomson relation, which describes the thermal influence on the liquid–solid interface evolution. The equation can be expressed as follows.[22,24]

$$\frac{v_n}{\mu_k} = T_m^0 - T - k_{GT}\kappa \tag{A1}$$

where μ_k is the kinetic coefficient, k_{GT} is the Gibbs–Thomson coefficient, v_n is the velocity of the interface, κ is the interface curvature gradient, and T_m^0 is the equilibrium melting temperature.

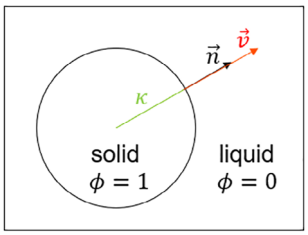

FIGURE A1 Solid–liquid interface representation

The normal to the interface is defined as $\vec{n} = -\frac{\nabla\phi}{|\nabla\phi|}$ (see Figure A1). Assume that $\phi(x, t)$ is a smooth Level Set function. Using the Level Set advection equation, we can write.

$$v_n = \vec{v}.\vec{n} = \frac{\partial x}{\partial t}\cdot\left(-\frac{\partial\phi/\partial x}{|\nabla\phi|}\right) = \frac{\partial\phi/\partial t}{|\nabla\phi|} \tag{A2}$$

By definition, the (total) curvature of the interface is given as:

$$\kappa = \nabla\cdot\vec{n} = -\frac{1}{|\nabla\phi|}\left[\nabla^2\phi - \frac{(\nabla\phi)\cdot\nabla|\nabla\phi|}{|\nabla\phi|}\right] \tag{A3}$$

By substituting Equations (A2) and (A3) in (A1) we find.

$$\frac{\partial\phi}{\partial t} = v_n|\nabla\phi| = \mu_k k_{GT}\left[\nabla^2\phi - \frac{(\nabla\phi)\cdot\nabla|\nabla\phi|}{|\nabla\phi|}\right] + \mu_k\left(T_m^0 - T\right)|\nabla\phi| \tag{A4}$$

In the Gibbs–Thomson equation, T_m^0 is considered as an equilibrium temperature T_e, that is, there is no evolution at this temperature.

For polymer material, at each crystallization temperature there is a specific crystallizable volume, since the amorphous phase has no melting temperature, the melting point of the polymer changes depending on its crystallization rate. Moreover, the crystallization is an exothermic process, using a perfect system without heat dissipation, the crystal will release its melting temperature. As a result, for polymer, the equilibrium temperature T_e is equal to T_m.

At equilibrium, $T = T_m$ and $\frac{\partial\phi}{\partial t} = 0$, Equation (A4) does not have a unique solution in the stationary case, for example, it depends on the initial profile. According to Beckermann et al.,[24] if a double-well potential is used for local free energy, the most commonly used profile for the steady state solution is given by:

$$\phi = \frac{1}{2}\left(1-\tanh\left(\frac{r}{2\delta}\right)\right) \tag{A5}$$

where 6δ is the interface thickness and r is the coordinate normal to the interface. According to Beckermann et al.[24], this is the most commonly used profile for a double-well free energy potential. Actually, depending on the choice of potential for the local free energy, the profile of the phase-field for the steady-state solution can be obtained through formal asymptotic analysis, and no assumption is needed.

Since evolution exists only in the normal direction of the interface, using Equation (A5), we can calculate:

$$|\nabla\phi| = \left|\frac{\partial\phi}{\partial r}\right| = \frac{\phi(1-\phi)}{\delta} \tag{A6}$$

$$\frac{(\nabla\phi)\cdot\nabla|\nabla\phi|}{|\nabla\phi|} = \nabla^2\phi = \frac{\partial^2\phi}{\partial r^2} = \frac{\phi(1-\phi)(1-2\phi)}{\delta^2} \tag{A7}$$

Equation (A4) becomes:

$$\begin{aligned}\frac{\partial\phi}{\partial t} &= \mu_k k_{GT}\left[\nabla^2\phi - \frac{\phi(1-\phi)(1-2\phi)}{\delta^2}\right] + \mu_k(T_m - T)\frac{\phi(1-\phi)}{\delta} \\ &= \mu_k k_{GT}\left[\nabla^2\phi - \frac{2}{\delta^2}\phi(1-\phi)\left(-\frac{\delta}{2k_{GT}}(T_m - T) + \frac{1}{2} - \phi\right)\right] \\ &= \mu_k k_{GT}\left[\nabla^2\phi - \frac{2}{\delta^2}\phi(1-\phi)\left(-m(T) + \frac{1}{2} - \phi\right)\right]\end{aligned} \tag{A8}$$

In Equation (A8), the term $\mu_k k_{GT}$ has dimension [m^2/s] and it represents the phase field diffusivity. Multiplying the diffusivity by $\frac{1}{\delta^2}$ we obtain the phase field mobility called M [s^{-1}], is also defined as a positive kinetic coefficient according to Allen–Cahn,[11] $1/M$ can be defined as a characteristic time of attachment of atoms at the interface according to Karma.[13] Taking $\epsilon^2 = \delta^2$ [m^2], ϵ is called the reference surface energy according to Cahn–Hilliard theory. To generalize the equation we replace a factor 2 with W which represents the energy barrier for second nucleation. Assume that $m(T) = \frac{\delta}{2k_{GT}}(T_m - T) = \gamma(T_m - T)$. After these approximations, Equation (A8) becomes:

$$\frac{\partial\phi}{\partial t} = M\left[\epsilon^2\nabla^2\phi - W\phi(1-\phi)\left(-m(T) + \frac{1}{2} - \phi\right)\right] \tag{A9}$$

Which can be rewritten as follows (proof in Appendix B):

$$\frac{\partial\phi}{\partial t} = M\left[\mathrm{div}\left(\epsilon^2\nabla\phi\right) - \frac{\partial f_{loc}}{\partial\phi}\right] = -M\frac{\delta F}{\delta\phi} \tag{A10}$$

Equation (A10) is similar to Allen–Cahn's[11] equation, where the total free energy F of the system of melt and solidifying crystals is defined as the Cahn–Hillard free energy:

$$F(\phi,T) = \int_V f_{loc}dV = \int_V \left[f_{liq-sol}(\phi,T) + f_{grad}(\phi)\right]dV \tag{A11}$$

With:

$$f_{liq-sol}(\phi,T) = W\int_0^\phi \phi(1-\phi)\left(-m(T) + \frac{1}{2} - \phi\right)d\phi \tag{A12}$$

And

$$f_{grad}(\phi) = \frac{1}{2}\epsilon^2(\nabla\phi)^2 \tag{A13}$$

If we consider that the reference surface energy ϵ is not a constant, then Equation (A10) becomes:

$$\frac{\partial\phi}{\partial t} = M\left[\nabla\cdot\left(\frac{1}{2}(\nabla\phi)^2\frac{\partial(\epsilon^2)}{\partial\nabla\phi}\right) + \nabla\cdot\left(\epsilon^2\nabla\phi\right) - W\phi(\phi-1)(\phi-1/2+m(T))\right] \tag{A14}$$

For two-dimensional model, it is assumed that the interface energy gradient ϵ is expressed as follows.[13]

$$\epsilon = \bar{\epsilon}[1 + \vartheta\cos(j(\theta-\theta_0))] \;|\; \theta = \arctan\left(\frac{\partial\phi/\partial y}{\partial\phi/\partial x}\right) \tag{A15}$$

where $\bar{\epsilon}$ is the reference interface energy gradient, ϑ is the strength of surface anisotropy, j is a shape parameter, θ is the angle between the interface normal and the reference axis and θ_0 is the spherulite orientation with respect to the horizontal axis, in this $\theta_0 = 0$.

Equation (A14) becomes.

$$\begin{aligned}\frac{1}{M}\frac{\partial\phi}{\partial t} = &-\frac{\partial}{\partial x}\left(\epsilon\epsilon'\frac{\partial\phi}{\partial y}\right) + \frac{\partial}{\partial y}\left(\epsilon\epsilon'\frac{\partial\phi}{\partial x}\right) \\ &+ \frac{\partial\epsilon^2}{\partial x}\frac{\partial\phi}{\partial x} + \frac{\partial\epsilon^2}{\partial y}\frac{\partial\phi}{\partial y} + \epsilon^2\left(\frac{\partial^2\phi}{\partial x^2} + \frac{\partial^2\phi}{\partial y^2}\right) \\ &- W\phi(\phi-1)(\phi-1/2+m(T))\end{aligned} \tag{A16}$$

where $\epsilon' = \partial\varepsilon/\partial\theta$.

Heat transfer equation

Suppose that we have two states (1 and 2). The enthalpy of the pure two phase body is determined as follows:

$$H = \phi_1 H_1 + \phi_2 H_2 \tag{A17}$$

where H_i is the enthalpy of the pure body in state i and ϕ_i is the volume fraction of phase i.

Assume $\phi = \phi_2$.

The enthalpy of change of state from phase 2 to phase 1 at temperature T $\Delta H_{2\rightarrow 1}$ also called latent heat, can be expressed as follows.

$$\Delta H_{2\rightarrow 1} = H_1 - H_2 \tag{A18}$$

Suppose that state 1 is liquid and 2 is solid. Using Equations (A17) and (A18) we obtain:

$$H = H_1 - \phi \Delta H_{2\rightarrow 1} = \rho C_p T - \rho L_f \phi \tag{A19}$$

where $\rho L_f = \Delta H_{2\rightarrow 1}$, L_f is the latent heat of fusion and C_p is the specific heat at constant pressure.

The heat transfer equation can be written as:

$$\frac{\partial H}{\partial t} = -\nabla . \vec{J} \tag{A20}$$

where $\vec{J} = -k_T \nabla T$ is the heat flow and k_T is the thermal conductivity.

Finally we get:

$$\rho C_p \frac{\partial T}{\partial t} = k_T \nabla^2 T + \rho L_f \frac{\partial \phi}{\partial t} \tag{A21}$$

Then we can write the equation system:

$$\begin{cases} \dfrac{\partial \phi}{\partial t} &= -M \dfrac{\delta F(m(T),\phi)}{\delta \phi} \\ \dfrac{\partial T}{\partial t} &= \alpha \nabla^2 T + K \dfrac{\partial \phi}{\partial t} \end{cases} \tag{A22}$$

where $\alpha = \frac{k_T}{\rho C_p}$ and $K = \frac{\Delta H_{2\rightarrow 1}}{\rho C_p}$.

APPENDIX B: NUMERICAL FORMULATION

In this Appendix, details are given about the finite difference method which was used to implement the proposed enhanced phase field model. Other methods exist in the literature, such as the variational formulations proposed by Valizadeh et al.[25] and Gomez et al.[26] for the Cahn–Hilliard model and based on isogeometric analysis.

Spatial discretization

The spatial gradient of the phase field variable is discretized as follows:

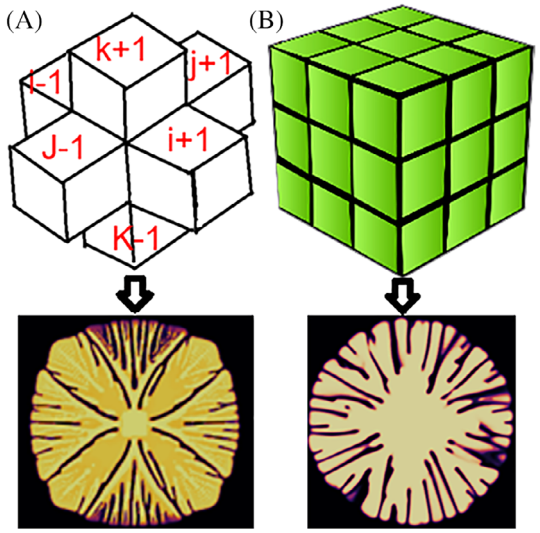

FIGURE B1 Influence on spherulite growth of the discretization of the spatial Laplacian operator using: (a) classical equation B.2 and (b) modified equation B.3

FIGURE B2 Illustration of periodic continuity conditions in 1D

$$\nabla \phi(x,y,z) \approx \begin{Bmatrix} \dfrac{\phi(x+\Delta x,y,z) - \phi(x-\Delta x,y,z)}{2\Delta x} \\ \dfrac{\phi(x,y+\Delta y,z) - \phi(x,y-\Delta y,z)}{2\Delta y} \\ \dfrac{\phi(x,y,z+\Delta z) - \phi(x,y,z-\Delta z)}{2\Delta z} \end{Bmatrix} \tag{B1}$$

The spatial Laplacian of the phase field variable is classically discretized as follows:

$$\nabla^2 \phi(x,y,z) \approx \begin{matrix} \dfrac{\phi(x+\Delta x,y,z) + \phi(x-\Delta x,y,z) - 2\phi(x,y,z)}{(\Delta x)^2} + \\ \dfrac{\phi(x,y+\Delta y,z) + \phi(x,y-\Delta y,z) - 2\phi(x,y,z)}{(\Delta y)^2} + \\ \dfrac{\phi(x,y,z+\Delta z) + \phi(x,y,z-\Delta z) - 2\phi(x,y,z)}{(\Delta z)^2} \end{matrix} \tag{B2}$$

However, the use of this classical expression generates an incorrect propagation of the interface and a distorted spherulite shape, as illustrated in Figure B1(A).

Therefore, we used a different discrete Laplacian expression. In order to motivate it, we assume for simplicity that $\Delta x = \Delta y = \Delta z = h$ and rewrite the classical expression as follows:

$$h^2 \nabla^2 \phi(x,y,z) \approx \phi(x+h,y,z) + \phi(x-h,y,z) + \phi(x,y+h,z) + \phi(x,y-h,z) + \phi(x,y,z+h) + \phi(x,y,z-h) - 6\phi(x,y,z)$$

We modify the classical formula so that it takes into account all the neighbors of a given element. This method is inspired by the work of Sanal.[27] Accordingly, the Laplacian of the phase field variable is computed as follows:

$$\begin{aligned}3h^2\nabla^2\phi(x,y,z)\approx\ &\phi(x+h,y,z)+\phi(x-h,y,z)+\\&\phi(x,y+h,z)+\phi(x,y-h,z)+\\&\phi(x,y,z+h)+\phi(x,y,z-h)+\\&\phi(x+h,y+h,z)+\phi(x-h,y-h,z)+\\&\phi(x,y+h,z+h)+\phi(x,y-h,z-h)+\\&\phi(x+h,y,z+h)+\phi(x-h,y,z-h)+\\&\phi(x+h,y-h,z)+\phi(x-h,y+h,z)+\\&\phi(x,y+h,z-h)+\phi(x,y-h,z+h)+\\&\phi(x+h,y,z-h)+\phi(x-h,y,z+h)+\\&\phi(x+h,y+h,z+h)+\phi(x-h,y-h,z-h)+\\&\phi(x+h,y-h,z-h)+\phi(x-h,y+h,z+h)+\\&\phi(x+h,y+h,z-h)+\phi(x-h,y-h,z+h)+\\&\phi(x-h,y+h,z-h)+\phi(x+h,y-h,z+h)-\\&26\phi(x,y,z)\end{aligned}\tag{B3}$$

The two Equations (B1) and (B3) are also used for the gradient and the Laplacian of the temperature field $T(x, y, z)$.

Time discretization

The time derivatives of the phase field and temperature variables at a given position (x, y, z) are approximated by the following discrete expressions:

$$\frac{\partial\phi}{\partial t}(t)\approx\frac{\phi(t+\Delta t)-\phi(t)}{\Delta t}\equiv\frac{\Delta\phi}{\Delta t}\tag{B4}$$

$$\frac{\partial T}{\partial t}(t)\approx\frac{T(t+\Delta t)-T(t)}{\Delta t}\equiv\frac{\Delta T}{\Delta t}\tag{B5}$$

However, in the heat Equation (A21), and following Kobayashi,[12] the discrete expression of the time derivative of the phase field variable is taken as follows:

$$\frac{\partial\phi}{\partial t}(t)\approx(1-\beta)\frac{\phi(t+\Delta t)-\phi(t)}{\Delta t}+\beta\frac{\phi(t)-\phi(t-\Delta t)}{\Delta t}\tag{B6}$$

where $\beta \in [0;1]$ is an integration parameter; in this work we take $\beta = 0.5$. The discrete expressions of $\nabla^2\phi$, $\nabla^2 T$, $\frac{\partial\phi}{\partial t}$, and $\frac{\partial T}{\partial t}$ are replaced in Equation (19) of the enhanced phase field model.

Boundary conditions

Conditions of periodic continuity are imposed on the border of the computational domain for both the temperature and the phase field variables. They can be illustrated with the simple 1D example with n_x elements depicted in Figure B2. The discrete spatial partial derivative $\phi_{,x}\approx\frac{\phi(n_x+1)-\phi(n_x-1)}{2\Delta x}$ becomes $\phi_{,x}\approx\frac{\phi(1)-\phi(n_x-1)}{2\Delta x}$ because by periodicity $\phi(n_x+1) = \phi(1)$.